

Block encoding with low gate count for second-quantized Hamiltonians

Diyi Liu,^{1,2} Shuchen Zhu,^{3,4,5} Lin Lin,^{1,6,7} Guang Hao Low,⁸ and Chao Yang¹

¹*Applied Mathematics and Computational Research Division,*

Lawrence Berkeley National Laboratory, Berkeley, California 94720, USA

²*Department of Mathematics, University of Minnesota, Minnesota 55455, USA*

³*Department of Mathematics, Duke University, Durham, North Carolina 27708, USA*

⁴*Duke Quantum Center, Duke University, Durham, North Carolina 27701, USA*

⁵*Department of Computer Science, Georgetown University, Washington, DC 20057, USA*

⁶*Department of Mathematics, University of California, Berkeley, California 94720, USA*

⁷*Challenge Institute of Quantum Computation, University of California, Berkeley, California 94720, USA*

⁸*Google Quantum AI, Venice, California 90291, USA*

(Dated: October 13, 2025)

Efficient block encoding of many-body Hamiltonians is a central requirement for quantum algorithms in scientific computing, particularly in the early fault-tolerant era. In this work, we introduce new explicit constructions for block encoding second-quantized Hamiltonians that substantially reduce Clifford+T gate complexity and ancilla overhead. By utilizing a data lookup strategy based on the SWAP architecture for the SPARSITY oracle O_C , and a direct sampling method for the AMPLITUDE oracle O_A with SELECT-SWAP architecture, we achieve a T count that scales as $\tilde{\mathcal{O}}(\sqrt{L})$ with respect to the number of interaction terms L in general second-quantized Hamiltonians. We also achieve an improved constant factor in the Clifford gate count of our oracle. Furthermore, we design a block encoding that directly targets the η -particle subspace, thereby reducing the sub-normalization factor from $\mathcal{O}(L)$ to $\mathcal{O}(\sqrt{L})$, and improving fault-tolerant efficiency when simulating systems with fixed particle numbers. Building on the block encoding framework developed for general many-body Hamiltonians, we extend our approach to electronic Hamiltonians whose coefficient tensors exhibit translation invariance or possess decaying structures. Our results provide a practical path toward early fault-tolerant quantum simulation of many-body systems, substantially lowering resource overheads compared to previous methods.

CONTENTS

I. Introduction	1	VII. Block encoding for η -particle Hamiltonian	17
II. Comparison with other input models	3	A. Indirect diffusion	17
A. Input model	3	B. State-dependent O_C and O_A oracles	18
B. Sparsity oracle	4	C. The implementation of O_{occ}	19
C. Amplitude oracle	4	D. The complete circuit for η -particle Hamiltonian	20
III. Preliminaries	5	VIII. Block encoding for structured Hamiltonian	22
A. Block encoding	5	A. Hamiltonians with nearest-neighbor interactions	23
B. Quantum signal processing and quantum singular value transformation	6	B. Hamiltonian with translation invariance	25
IV. Sparsity oracle O_C	6	C. Hamiltonians that can be factorized as products of number operators	27
A. Second-quantized Hamiltonian	7	D. Examples	27
B. Representation of many-body state and many-body Hamiltonian	7	1. Nearest-neighbor Hubbard model	27
C. Oracle construction	9	2. Molecular Electronic Hamiltonian with localized orbitals	29
1. One-body interactions	9	3. Extended Hubbard model	30
2. Number operator	11	IX. Conclusion and future work	30
3. Two-body interactions	11	Acknowledgments	31
4. Beyond two-body interaction	12	References	31
V. Amplitude oracle O_A	12		
A. Data-lookup oracle	13		
B. Direct sampling method	14		
C. Oracle construction	15		
VI. The complete circuit for general Hamiltonians	15		

I. INTRODUCTION

Quantum algorithms for simulating many-body systems require efficient encoding of non-unitary operators

(a) Full Hilbert space (no particle-number constraint).

Model	Reference	Qubit	Subnormalization factor	T count	T depth
General	Babbush et al. (2018) [1]	$\mathcal{O}(n + \log(\frac{n^4}{\epsilon}))$	$\mathcal{O}(n^4)$	$\mathcal{O}(n^4 + \log(\frac{n^4}{\epsilon}))$	$\mathcal{O}(n^4)$
	This work	$\mathcal{O}(n^2 \sqrt{\log(\frac{n^4}{\epsilon}))})$	$\mathcal{O}(n^4)$	$\mathcal{O}(n^2 \sqrt{\log(\frac{n^4}{\epsilon}))})$	$\mathcal{O}(n^2 \sqrt{\log(\frac{n^4}{\epsilon}))})$
Factorized	Kivlichan et al. (2018) [2]	N/A	N/A	$\mathcal{O}(n^2 \log(\frac{1}{\epsilon}))$	$\mathcal{O}(n)$
TI Factorized	Babbush et al. (2018) [1]	$\mathcal{O}(n + \log(\frac{n^2}{\epsilon}))$	$\mathcal{O}(n^2)$	$\mathcal{O}(n + \log(\frac{n^2}{\epsilon}))$	$\mathcal{O}(n)$
	This work	$\mathcal{O}(n + \sqrt{n \log(\frac{n^2}{\epsilon}))})$	$\mathcal{O}(n^2)$	$\mathcal{O}(n + \sqrt{n \log(\frac{n^2}{\epsilon}))})$	$\mathcal{O}(\sqrt{n \log(\frac{n^2}{\epsilon}))})$
Localized	Wan (2021) [3]	$\mathcal{O}(n)$	$\mathcal{O}(n^2)$	$\mathcal{O}(n) + \text{PREP}$	$\mathcal{O}(n) + \text{PREP}$
	This work	$\tilde{\mathcal{O}}(n \sqrt{\log^3(\frac{n^2}{\epsilon}))})$	$\mathcal{O}(n^2 \log^2(\frac{n^2}{\epsilon}))$	$\tilde{\mathcal{O}}(n \sqrt{\log^3(\frac{n^2}{\epsilon}))})$	$\tilde{\mathcal{O}}(n \sqrt{\log^3(\frac{n^2}{\epsilon}))})$

(b) Fixed η -particle subspace.

Model	Reference	Qubit	Subnormalization factor	T count	T depth
General	Babbush et al. (2018) [1]	$\mathcal{O}(n + \log(\frac{n^4}{\epsilon}))$	$\mathcal{O}(n^4)$	$\mathcal{O}(n^4 + \log(\frac{n^4}{\epsilon}))$	$\mathcal{O}(n^4)$
	This work	$\mathcal{O}(n^2 \sqrt{\log(\frac{n^2 \eta^2}{\epsilon}))})$	$\mathcal{O}(n^2 \eta^2)$	$\mathcal{O}(n^2 \sqrt{\log(\frac{n^2 \eta^2}{\epsilon}))})$	$\mathcal{O}(n^2 \sqrt{\log(\frac{n^2 \eta^2}{\epsilon}))})$
Factorized	Kivlichan et al. (2018) [2]	N/A	N/A	$\mathcal{O}(n^2 \log(\frac{1}{\epsilon}))$	$\mathcal{O}(n)$
TI Factorized	Babbush et al. (2018) [1]	$\mathcal{O}(n + \log(\frac{n^2}{\epsilon}))$	$\mathcal{O}(n^2)$	$\mathcal{O}(n + \log(\frac{n^2}{\epsilon}))$	$\mathcal{O}(n)$
	This work	$\mathcal{O}(n + \sqrt{n \log(\frac{n \eta}{\epsilon}))})$	$\mathcal{O}(n \eta)$	$\mathcal{O}(n \log(\eta) + \sqrt{n \log(\frac{n \eta}{\epsilon}))})$	$\mathcal{O}(n \log(\eta) + \sqrt{n \log(\frac{n \eta}{\epsilon}))})$
Localized	Wan (2021) [3]	$\mathcal{O}(n)$	$\mathcal{O}(n^2)$	$\mathcal{O}(n) + \text{PREP}$	$\mathcal{O}(n) + \text{PREP}$
	This work	$\tilde{\mathcal{O}}(n + \eta \sqrt{\log^3(\frac{n^2}{\epsilon}))})$	$\mathcal{O}(\eta^2 \log^2(\frac{n^2}{\epsilon}))$	$\tilde{\mathcal{O}}(n \log(\eta) + \eta \sqrt{\log^3(\frac{n^2}{\epsilon}))})$	$\tilde{\mathcal{O}}(n \log(\eta) + \eta \sqrt{\log^3(\frac{n^2}{\epsilon}))})$

TABLE I: Complexity of input models for electronic structure Hamiltonians. Here n is the number of spin orbitals, η is the particle number, and ϵ is the target precision. $\tilde{\mathcal{O}}$ hides polylogarithmic factors in n and ϵ . PREP refers to the cost of the PREPARE oracle, and N/A means not applicable.

into quantum circuits [4–6]. One widely used framework for this purpose is block encoding, which embeds a scaled non-unitary matrix into a larger unitary that can be implemented on a quantum computer [7, 8]. The idea of embedding operators into unitaries has roots in early Hamiltonian simulation algorithms, where oracles or direct matrix exponentiation methods were used to simulate sparse Hamiltonians [9, 10]. The development of quantum singular value transformation (QSVT) and quantum signal processing (QSP) later provided a systematic way to manipulate encoded operators with near-optimal resource overhead [8, 11].

Although there has been rich progress on the block encoding and it is now regarded as an essential tool in quantum algorithm design [12, 13], most prior works focus either on reducing CNOT gate count for noisy intermediate-scale quantum (NISQ) devices or on algorithm design under the assumption of fully fault-tolerant quantum computers [14]. Constructing explicit and resource-efficient circuits tailored for early fault-tolerant architectures remains a substantial challenge. This is particularly true for many-body systems, where the underlying operators often have complicated structures and

large norms that make direct implementation costly. Optimizing block encoding constructions for realistic quantum hardware, minimizing gate counts, and reducing ancilla overhead are important steps toward making quantum simulation algorithms practical in the near term [1].

Input models specify how classical data—such as sparse matrices [15, 16] and kernel matrices [17], matrix product operators [18], partial differential operators [19–23], physical Hamiltonians of quantum systems [24–28], or pseudo-differential operators [29]—are encoded and made accessible to quantum computers [30, 31]. A standard framework for building input models is called the *linear combination of unitaries* (LCU) method [1, 32]. In LCU, a Hamiltonian is decomposed as a sum of simpler unitary operators, each with an associated weight. Two oracles are required: the PREPARE oracle prepares a quantum state encoding the coefficients of the unitary terms, and the SELECT oracle conditionally applies a unitary based on an index in a quantum register. Together, they provide a principal way to access and manipulate the Hamiltonian, making them central to many quantum algorithms. This approach can also be referred to as *block encoding*.

The block encoding proposed in this work shares structural similarities with input models based on SELECT and PREPARE oracles. While block encoding has roots in qubitization [11, 33] and related ideas for representing sparse matrices in *numerical linear algebra* [34, 35], our approach differs fundamentally from LCU-type constructions. In LCU methods, the implementation depends on the specific unitary decomposition, whereas our block encoding emphasizes the choice of basis for sparse matrix representation of the Hamiltonian and is based on embedding rather than decomposition.

For a second-quantized Hamiltonian with L terms, standard block encoding methods incur a T gate cost that scales at least linearly in L , even with techniques such as alias sampling [1]. This overhead is especially inefficient when the Hamiltonian commutes with the total number operator and only the fixed-particle subspace is relevant. Designing block encodings that act directly on this subspace while reducing the subnormalization factor remains an open problem [36, 37], motivating new approaches that lower T gate counts and target the physically relevant sector.

In this work, we develop an efficient block encoding scheme for general second-quantized Hamiltonians that addresses the aforementioned challenges. Our construction reduces the T gate count from linear to sublinear scaling in the number of terms L , achieving a complexity of $\tilde{\mathcal{O}}(\sqrt{L})$. The approach combines data lookup techniques for implementing the SPARSITY oracle O_C , which specifies the nonzero entries of the Hamiltonian, with direct sampling strategies for the AMPLITUDE oracle O_A , which encodes the corresponding coefficients. This leads to a significant reduction in overall resource cost, as summarized in Table I.

In addition, inspired by [36], we design a block encoding that targets the η -particle subspace directly, reducing the *subnormalization factor* from $\mathcal{O}(L)$ to $\mathcal{O}(\sqrt{L})$ for second-quantized Hamiltonians with one-body interaction and two-body interaction. In the context of block encoding, the subnormalization factor is defined as the scaling constant $\alpha \geq |H|$ such that the unitary U satisfies $\langle 0|U|0\rangle = H/\alpha$, where H is the target Hamiltonian. The computational cost of simulating time-independent quantum dynamics e^{-iHt} on a quantum computer scales linearly with α . Consequently, designing block encodings with a smaller subnormalization factor directly results in more resource-efficient quantum simulation algorithms. Although this work primarily focuses on constructing block encodings for Hamiltonians with up to two-body interactions, we note that our scheme naturally generalizes to more complex Hamiltonians, such as those in nuclear many-body physics [25, 26] and quantum chromodynamics. These improvements make block encoding more practical for early fault-tolerant quantum devices, especially for electronic structure simulations where second quantization is the natural formulation. Prior work on first-quantized approaches has embraced a similar philosophy [38, 39]. However, when many-body phenomena

are naturally expressed in the second-quantized formalism and cannot be easily translated into first quantization [40], it remains unclear how to construct suitable input models for simulation in a first-quantized manner. While there has been some progress using pseudo-potentials in first quantization [41], there is still no rigorous mathematical understanding of how accurately electronic structure can be computed from such models.

We benchmark our method against prior input models in Sec. II, highlighting its superior performance in terms of gate counts, circuit depth, and fault-tolerant resource requirements through the use of the SPARSITY and AMPLITUDE oracle constructions. We introduce the fundamental concepts used throughout the paper in Sec. III.

The construction of the SPARSITY oracle O_C for one-body and two-body interactions in second-quantized many-body Hamiltonians is presented in Sec. IV, where we analyze the resource cost of constructing explicit circuits for encoding fermionic operators. In Sec. V, we present a new method for constructing the AMPLITUDE oracle O_A with two subroutines: a data lookup oracle using the SELECT-SWAP circuit and a direct sampling oracle. We show how these two oracles efficiently encode the amplitudes corresponding to the Hamiltonian coefficients. An optimized block encoding strategy targeted at the η -particle Hamiltonian is introduced in Sec. VII. We discuss a state-dependent AMPLITUDE oracle O_A tailored for fixed-particle-number subspaces and describe the occupation detection oracle for coefficient preparation. We then apply these techniques to concrete physical models in Sec. VIII D, including the Hubbard model, electronic structure Hamiltonians, and interacting models for 2D materials. We provide explicit resource estimates demonstrating the improvements.

We summarize the contributions of the paper and outline potential directions for future research in Sec. IX.

II. COMPARISON WITH OTHER INPUT MODELS

In this section, we give an introduction of input model and compare our block encoding with the alternative input models from prior work. Instead of the traditional framework based on the SELECT and PREPARE oracles, we frame the discussion in terms of the SPARSITY and AMPLITUDE oracles, which serve as their respective replacements in our construction. We then compare the overall gate complexity and subnormalization factor against previous approaches.

A. Input model

Many quantum simulation algorithms focus on estimating the properties of a specific Hamiltonian, typically formulated as queries to oracles that encode the Hamiltonian in some form. Such oracles are known as *input*

model and can generally be decomposed into two components, namely PREPARE oracle and SELECT oracle.

One way to build input models is the LCU method [1, 32], which works for Hamiltonians that can be decomposed into a summation of a sequence of unitary operators. Consider one such Hamiltonian $\mathcal{H} = \sum_{i=0}^{L-1} \alpha_i \mathcal{H}_i$, $\alpha_i > 0$ be the linear combination of unitary matrices \mathcal{H}_i .

The SELECT oracle is defined as

$$\text{SELECT} := \sum_{i \in [L]} |i\rangle \langle i| \otimes \mathcal{H}_i, \quad (1)$$

and it implements the selection of \mathcal{H}_i conditioned on the value of the log L -qubit ancilla states (also called the control register). It satisfies that given a state $|\psi\rangle$,

$$\text{SELECT} |i\rangle |\psi\rangle = |i\rangle \mathcal{H}_i |\psi\rangle. \quad (2)$$

The PREPARE oracle is a unitary operation satisfying

$$\text{PREPARE} |0^{\log L}\rangle = \frac{1}{\sqrt{\|\alpha\|_1}} \sum_{i \in [L]} \sqrt{\alpha_i} |i\rangle. \quad (3)$$

The l_1 -norm of the coefficients is given by $\|\alpha\|_1 = \sum_i |\alpha_i|$. Together, they form the standard block encoding via

$$\text{PREPARE} \rightarrow \text{SELECT} \rightarrow \text{PREPARE}^\dagger. \quad (4)$$

Lemma II.1 (LCU). *Define*

$$W = (\text{PREPARE}^\dagger \otimes I_n) \text{ SELECT} (\text{PREPARE} \otimes I_n), \quad (5)$$

then for any $|\psi\rangle$,

$$W |0^{\log L}\rangle |\psi\rangle = \frac{1}{\|\alpha\|_1} |0^{\log L}\rangle \mathcal{H} |\psi\rangle + |\tilde{\perp}\rangle, \quad (6)$$

where $|\tilde{\perp}\rangle$ is an unnormalized state satisfying $(|0^{\log L}\rangle \langle 0^{\log L}| \otimes I_n) |\tilde{\perp}\rangle = 0$. In other words, W is a $(\|\alpha\|_1, \log L)$ -block-encoding of \mathcal{H} .

The input model introduced above does not specify how the circuits are built in practice, but only illustrates the high-level structure of the model. Practical construction of these oracles would use extra ancilla qubits, and \mathcal{H}_i can be non-unitaries. For example, Hamiltonians or sparse matrices commonly used in quantum chemistry, quantum materials, or quantum field theory, the intrinsic decomposition term \mathcal{H}_i may not be unitary. In this case, it must be embedded in a unitary U_i , whose linear combination yields the block encoding of \mathcal{H} , at the cost of additional ancilla qubits. To resolve this issue, a series of works [8, 24, 42] were done to efficiently construct block encodings of sparse matrices. In this framework, an AMPLITUDE oracle O_A is used to encode the values of nonzero matrix elements, and a SPARSITY oracle O_C is used to encode the positions of these matrix elements. The structure of block encoding follows as

$$D_s \rightarrow O_A \rightarrow O_C \rightarrow D_s, \quad (7)$$

where D_s is a diffusion operator, constructed through a sequence of Hadamard gates.

B. Sparsity oracle

The SPARSITY oracle O_C allows the controlled application of Hamiltonian terms within block-encoding frameworks such as qubitization, quantum walks, and QSP. For second-quantized Hamiltonians, the SPARSITY oracle O_C captures the sparsity structure of the Hamiltonian matrix and encodes it in a unitary form suitable for quantum computation. Since quantum circuits can only implement unitary operations, a non-unitary Hamiltonian must first be expressed as a linear combination of unitaries—for example, as sums of Pauli strings or products of creation and annihilation operators for Majorana fermions. Different choices of decomposition correspond to different implementations of the O_C oracle.

The O_C oracle implements the mapping

$$O_C |\ell\rangle |j\rangle := |\ell\rangle |c(j, \ell)\rangle, \quad (8)$$

where $c(j, \ell)$ is the ℓ -th non-zero entry in column j of \mathcal{H} . A direct implementation uses controlled unitaries, for instance sequences of controlled-Pauli gates [24]. This can be improved by more efficient constructions of multi-qubit control [1], which reduce the gate cost from $\mathcal{O}(n \log(n))$ to $\mathcal{O}(n)$. In contrast, our approach avoids a controlled unitary for every ℓ and instead employs a SWAP network (detail in Sec. IV) to realize the O_C oracle, following the method of [43], which has also been applied in the Jordan–Wigner setting [3].

Our method is the first to apply both the SWAP network and the concept of block encoding to construct an O_C oracle for a general second-quantized Hamiltonian, as well as for the η -particle subspace of the Hamiltonian. We note that the O_C oracle achieves a gate count of $\mathcal{O}(n)$, matching the best-known results. Compared to the Jordan–Wigner-based method [3], our construction has a smaller constant overhead in both gate count and circuit depth. This improvement comes from the fact that the number of terms in the decomposition-based input model is only a constant multiple of that in the embedding-based model.

C. Amplitude oracle

The O_A oracle generates quantum states of the form

$$O_A |0\rangle |\ell\rangle |j\rangle := \left(\mathcal{H}_{c(j, \ell), j} |0\rangle + \sqrt{1 - |\mathcal{H}_{c(j, \ell), j}|^2} |1\rangle \right) |\ell\rangle |j\rangle. \quad (9)$$

A direct implementation uses L multi-qubit controlled rotations to encode the amplitudes $\sqrt{\rho_i}$. However, this construction incurs an additional subnormalization factor of $\mathcal{O}(L)$, since it relies on a sequence of Hadamard gates [15, 24]. Such an extra subnormalization factor leads to a worse simulation gate cost. Several methods have been proposed to remove such a subnormalization factor in O_A oracles.

A notable example is the *divide-and-conquer* (tree-based) scheme for arbitrary state preparation [44, 45], which uses $\mathcal{O}(L \log(L))$ T gates. With further depth optimization, it has been shown that arbitrary n -qubit, L -sparse states can be prepared with circuit depth $\Theta(\log(nL))$ using $\mathcal{O}(nL \log(L))$ qubits [46]. For general second-quantized Hamiltonians, however, it remains unclear whether such methods can achieve gate cost sublinear in L .

Another approach removes the $\mathcal{O}(L)$ subnormalization factor by applying *alias sampling* with extra ancilla qubits [1, 47, 48], but this cannot be directly used to build the O_A oracle for the η -particle subspace of a general second-quantized Hamiltonian. The method of [1] is a special case of the data-lookup oracle of [43], which we also adopt. Our construction lowers the gate cost from $\mathcal{O}(L)$ to $\tilde{\mathcal{O}}(\sqrt{L})$.

In certain cases, the cost of constructing the O_A oracle can be further reduced. When the Hamiltonian coefficients come from smooth functions, the state can be prepared with $\mathcal{O}(\log(L))$ gates [49]; if they admit a matrix-product structure, preparation is possible with $\mathcal{O}(\log(L))$ depth [50]. We also note recent progress in the parallel application of QROM using mass-production techniques [51].

III. PRELIMINARIES

We use Dirac notation $\langle \cdot |$ and $|\cdot \rangle$ to represent row and column vectors, respectively. Specifically, $|0\rangle$ and $|1\rangle$ are used to denote the unit vectors $e_0 = [1 \ 0]^T$ and $e_1 = [0 \ 1]^T$. The tensor product of m $|0\rangle$'s is written as $|0^m\rangle$. We use $|x, y\rangle$ to represent the Kronecker product of $|x\rangle$ and $|y\rangle$, which can also be written as $|x\rangle|y\rangle$ or $|xy\rangle$. The $N \times N$ identity matrix is denoted by I_N , and we may omit the subscript N when the dimension is clear from the context.

We map the binary representation of an integer $l \in \mathbb{N}$ where $0 \leq l \leq 2^n - 1$,

$$l = l_0 \cdot 2^0 + l_1 \cdot 2^1 + \cdots + l_{n-1} \cdot 2^{n-1},$$

with $l_i \in \{0, 1\}$ for $i = 0, 1, 2, \dots, n-1$, to a quantum state $|l\rangle$, often written as $|l_0, \dots, l_{n-1}\rangle$. The superposition of these states can be encoded using n qubits, where $|l\rangle$ corresponds to the i th qubit.

We use H , X , Y , and Z to denote the Hadamard, Pauli- X , Pauli- Y , and Pauli- Z matrices, respectively. We adhere to the standard convention for drawing quantum circuits, which feature multiple parallel lines intersected by several layers of rectangular boxes. Each line represents either a single qubit or multiple qubits, depending on its label, and each box represents a single-qubit or multi-qubit gate, depending on how many qubit lines pass through it. Qubits in a circuit diagram are numbered in increasing order from top to bottom, as shown in the 3-qubit circuit U in Fig. 1. An integer

$l = [l_{n-1} \dots l_1 l_0]$ input to a circuit is prepared as a quantum state $|l_0 \dots l_{n-1}\rangle$, with $|l_0\rangle$ mapped to the 0-th qubit and $|l_{n-1}\rangle$ mapped to the $(n-1)$ -th qubit.

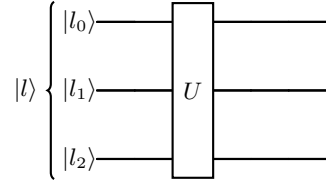


FIG. 1: Illustration of the circuit convention.

A. Block encoding

Block encoding [33] is a technique for embedding a properly scaled non-unitary matrix $A \in \mathbb{C}^{N \times N}$ into a unitary matrix U_A of the form

$$U_A = \begin{bmatrix} A & * \\ * & * \end{bmatrix}. \quad (10)$$

Applying U_A to a vector of the form

$$v = \begin{bmatrix} x \\ 0 \end{bmatrix} = |0\rangle|x\rangle, \quad (11)$$

yields

$$w = U_A v = \begin{bmatrix} Ax \\ * \end{bmatrix} = |0\rangle(A|x\rangle) + |1\rangle|*\rangle. \quad (12)$$

If the first qubit is measured and the $|0\rangle$ state is obtained, the second qubit register then contains $A|x\rangle$, with the probability of such a measurement being $\|A|x\rangle\|^2$. A formal definition of block encoding is as follows.

Definition III.1 (Block encoding). *Given an n -qubit matrix $A \in \mathbb{C}^{2^n \times 2^n}$, if for some $\alpha, \varepsilon \in \mathbb{R}_+$, and an $(m+n)$ -qubit unitary matrix U_A so that*

$$\|A - \alpha(|0^m\rangle \otimes I_{2^n})U_A(|0^m\rangle \otimes I_{2^n})\| \leq \varepsilon, \quad (13)$$

then U_A is called an (α, m, ε) -block-encoding of A . When the block encoding is exact with $\varepsilon = 0$, U_A is called an (α, m) -block-encoding of A .

Given that U_A can be represented by a quantum circuit, a quantum computer can produce $|Ax\rangle$ by measuring the ancilla qubits.

The following theorem outlines a general method for constructing a block encoding of an s -sparse matrix, which is defined as a matrix with no more than s nonzero elements in each column (see [8, 15, 24]).

Theorem III.2. *Let $c(j, \ell)$ be a function that gives the row index of the ℓ th (among a list of s) non-zero matrix elements in the j th column of an s -sparse matrix $A \in$*

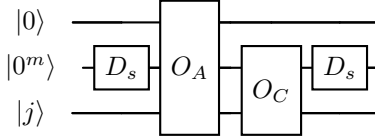


FIG. 2: A schematic illustration of a quantum circuit for the block encoding of an s -sparse matrix.

$\mathbb{C}^{N \times N}$ with $N = 2^n$, where $s = 2^m$. We denote the (i, j) th element of A by $A_{i,j}$. If there exists a unitary O_c (SPARSITY oracle) such that

$$O_c |\ell\rangle |j\rangle = |\ell\rangle |c(j, \ell)\rangle, \quad (14)$$

and a unitary O_A (AMPLITUDE oracle) such that

$$O_A |0\rangle |\ell\rangle |j\rangle = \left(A_{c(j, \ell), j} |0\rangle + \sqrt{1 - |A_{c(j, \ell), j}|^2} |1\rangle \right) |\ell\rangle |j\rangle, \quad (15)$$

then

$$U_A = (I_2 \otimes D_s \otimes I_N) (I_2 \otimes O_c) O_A (I_2 \otimes D_s \otimes I_N), \quad (16)$$

block encodes A/s . Here D_s is called a diffusion operator and is defined as

$$D_s \equiv \underbrace{H \otimes H \otimes \cdots \otimes H}_m, \quad (17)$$

The basic structure of the block encoding circuit is shown in Fig. 2. Note that the input to the circuit consists of three sets of qubits. The top qubit is used to encode nonzero matrix elements. The second set of qubits that takes $|0^m\rangle$ as the input is used to encode the position of the nonzero elements. The bottom set of qubits that take $|j\rangle$ as the input are the qubits that encode the column indices of the matrix to be block encoded.

The circuit consists of several blocks. The O_C block is used to encode the positions of the nonzero elements, which is defined by the mapping $c(j, \ell)$ in Theorem III.2. The O_A block is used to encode the nonzero matrix elements.

The circuit structure of O_C depends on the mapping $c(j, \ell)$, which describes the sparsity structure of A . Ref. [15] showed how $c(j, \ell)$ is defined for tridiagonal Toeplitz matrices and sparse matrices whose sparsity structure can be described by a binary tree, as well as how the O_C circuit can be constructed efficiently for those types of matrices.

Once O_C is specified, we can construct O_A , which encodes the numerical value of each non-zero matrix element.

B. Quantum signal processing and quantum singular value transformation

In this section, we introduce quantum signal processing and quantum singular value transformation to show

how block encoding can be used for solving linear algebra problems and scientific computing. To solve the linear algebra problems involving A or compute physical observables, one needs to block encode a matrix function of A . Quantum signal processing [52] (QSP) for scalar polynomials and its extension to matrix polynomials through the quantum singular value transformation [33] (QSVT) enable access to the block encoding of a matrix polynomial of A based on the block encoding of A .

Theorem III.3 (Quantum signal processing). *Let*

$$U(t) = \begin{bmatrix} t & \sqrt{1-t^2} \\ \sqrt{1-t^2} & -t \end{bmatrix}, \quad (18)$$

where $|t| \leq 1$. There exists a set of phase angles $\Phi_d \equiv \{\phi_0, \dots, \phi_d\} \in \mathbb{R}^{d+1}$ so that

$$\begin{aligned} U_{\Phi_d}(t) &\equiv (-i)^d e^{i\phi_0 Z} \prod_{j=1}^d [U(t) e^{i\phi_j Z}] \\ &= \begin{bmatrix} p(t) & -q(t)\sqrt{1-t^2} \\ q^*(t)\sqrt{1-t^2} & p^*(t) \end{bmatrix}, \end{aligned} \quad (19)$$

if and only if $p(t)$ and $q(t)$ are complex valued polynomials in t and satisfy

1. $\deg(p) \leq d$, $\deg(q) \leq d-1$;
2. p has parity d mod 2, and q has parity $d-1$ mod 2;
3. $|p(t)|^2 + (1-t^2)|q(t)|^2 = 1$, $\forall t \in [-1, 1]$.

When $d = 0$, $\deg(q) \leq -1$ should be interpreted as $q = 0$.

Note that $U_{\Phi_d}(t)$ is a block encoding of the function p of a scalar t in Theorem III.3. This theorem can be extended to a properly scaled matrix, which is the theory behind QSVT.

It follows from QSVT that the block encoding of $p(A)$ for some polynomial p can be expressed in terms of the block encoding of A , as illustrated in Fig. 3. In the circuit representation, ϕ_i is the same phase angle appearing in Theorem III.3. Each controlled-rotation gate CR_{ϕ_i} can be implemented as a single-qubit gate placed on the top ancilla qubit that performs $e^{-i\phi_i Z}$, preceded and followed by a multi-qubit CNOT gate.

While Theorem III.3 asserts the existence of these phase angles for quantum signal processing, they can be effectively computed through solving a numerical optimization problem as detailed in Refs. [53, 54].

IV. SPARSITY ORACLE O_C

We start the section by introducing the second-quantized Hamiltonian, a widely used model for quantum chemistry, condensed matter physics, and nuclear physics. Then we explain the way we encode our quantum many-body wave in Eq. (24) on the quantum computer. At the end of the section, we introduce the O_C oracle designed in the paper and estimate the cost.

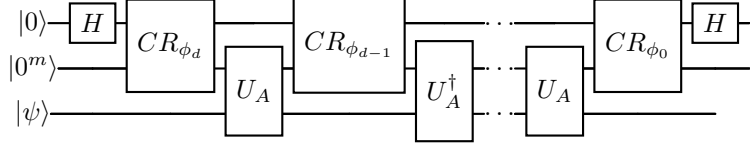


FIG. 3: Illustration: the schematic circuit design of quantum singular value transformation (for an odd d ; for an even d the last U_A is replaced by U_A^\dagger). The additional Hadamard gate selects only the real part of the polynomial p .

A. Second-quantized Hamiltonian

The second-quantized many-body Hamiltonian, as shown in Eq. (20)

$$\mathcal{H} = \sum_{p,q} h_{pq} a_p^\dagger a_q + \sum_{p < q, r < s} h_{pqrs} a_p^\dagger a_q^\dagger a_r a_s, \quad (20)$$

arises in quantum chemistry and nuclear physics, where h_{pq} and h_{pqrs} denote the strength parameters that correspond to the one-body and two-body interactions of the electrons or nucleons. a_p^\dagger and a_q are the fermionic creation and annihilation operators, with the index p, q labeling a single-fermion state. For fermions, the creation and annihilation operators satisfy the following anti-commutation relations:

$$\{a_p, a_q^\dagger\} = \delta_{pq}, \quad (21)$$

and

$$\{a_p, a_q\} = \{a_p^\dagger, a_q^\dagger\} = 0. \quad (22)$$

Here, $\{\hat{a}, \hat{b}\} = \hat{a}\hat{b} + \hat{b}\hat{a}$ denotes the anti-commutator. As with the bosonic case, the delta function δ_{pq} ensures that the anti-commutator is non-zero only when $p = q$.

B. Representation of many-body state and many-body Hamiltonian

In the subsection, we introduce the formalism we use to represent a quantum many-body basis state and the matrix representation of a second-quantized many-body Hamiltonian in a set of such basis states.

Because the Hamiltonian we consider in Eq. (20) is particle number conserved, i.e., \mathcal{H} commutes with number operator $\mathcal{N} = \sum_i a_i^\dagger a_i$, we can consider the invariant subspace of \mathcal{H} associated with η -particle states $|j\rangle$ that satisfies $\mathcal{N}|j\rangle = \eta|j\rangle$ for some $\eta \in \mathbb{N}$. The occupation representation of such a state $|j\rangle \equiv |j_0 j_1 \dots j_{n-1}\rangle$, where n is the total number of single-particle states from which the η -particles are chosen and $j_0 j_1 \dots j_{n-1}$, with $j_i \in \{0, 1\}$, is the binary representation of j , satisfies

$$\begin{cases} j_i = 1 & \text{for integers } i = f_0, f_1, \dots, f_{\eta-1}, \\ j_i = 0 & \text{for other integers } i \in [0, n-1], \end{cases} \quad (23)$$

where $0 \leq f_0 < f_1 < \dots < f_{\eta-1} \leq n-1$ are a set of integers between 0 and $n-1$. Such an η -particle state can alternatively be represented as

$$a_{f_0}^\dagger a_{f_1}^\dagger \dots a_{f_{\eta-1}}^\dagger |vac\rangle, \quad (24)$$

where $|vac\rangle$ represents the empty or vacuum state. Note that Eq. (24) is only valid when $f_0, f_1, \dots, f_{\eta-1}$ is an increasing integer sequence. When this is not true, we can use the anti-commutation identity Eq. (22) to repeatedly interchange the order of two adjacent out-of-order creation operators indexed by different f_k 's until the indices of reordered creation operators become an increasing sequence. Every time we invoke the anti-commutation identity, we introduce a negative sign. The final sign of the created many-body basis state depends on the number of reordering performed, i.e., Eq. (24) may produce $-|j\rangle$ for some many-body basis state $|j\rangle$. For example, $a_2^\dagger a_1^\dagger |vac\rangle$ is not a valid many-body basis state. However, it is a many-body basis multiplied by -1 because

$$a_2^\dagger a_1^\dagger |vac\rangle = -a_1^\dagger a_2^\dagger |vac\rangle := -|011\rangle. \quad (25)$$

The occupation representation of the $|j\rangle$ basis state can be mapped directly to a n -qubit register with $|j_p\rangle$ mapped to the p th qubit. The representation defined by Eq. (24) is convenient when we examine the state resulting from the application of a set of creation and annihilation operators to $|j\rangle$.

The matrix representation of \mathcal{H} can be obtained by evaluating $\mathcal{H}_{i,j} \equiv \langle i | \mathcal{H} | j \rangle$ for all i, j pairs, where $i, j \in 0, 1, \dots, 2^n - 1$. For the two-body \mathcal{H} defined in Eq. (20), many of these matrix elements are zero. In particular, $\langle i | \mathcal{H} | j \rangle = 0$, if $|i\rangle$ and $|j\rangle$ differ by more than two single particle states.

The nonzero structure of the matrix representation of \mathcal{H} can be ascertained by examining the state $\mathcal{H}|j\rangle$ is in for each j . Because the two-body Hamiltonian \mathcal{H} defined in Eq. (20) is a linear combination of one-body operator $a_p^\dagger a_q$ and two-body operators $a_p^\dagger a_q^\dagger a_r a_s$, for $p, q, r, s \in \{0, 1, \dots, n-1\}$, it is sufficient to examine basis states produced when each one of these operators is applied to $|j\rangle$ to deduce the position i of the nonzero matrix in column j of the matrix \mathcal{H} . The value of the nonzero matrix element depends on the coefficients h_{pq} and h_{pqrs} in Eq. (20), which we will discuss later.

For simplicity, let us first look at basis states produced from applying $a_p^\dagger a_q$ to $|j\rangle$. We note that

- $a_p^\dagger a_q$ may not contribute to a nonzero matrix element in the j th column of \mathcal{H} . This is because $a_p^\dagger a_q |j\rangle = 0 |vac\rangle = 0$ if $|j\rangle_p = 1$ or $|j\rangle_q = 0$, where $|j\rangle_p$ denotes the occupation number of the p th single particle state in $|j\rangle$.
- $a_p^\dagger a_q$ contributes to a nonzero element of in the j th column of \mathcal{H} if $|j\rangle_p = 0$ and $|j\rangle_q = 1$.
- When $|j\rangle_p = 0$ and $|j\rangle_q = 1$,

$$a_p^\dagger a_q |j\rangle = (-1)^{d_{j,p,q}} |\text{FLIP}(j; p, q)\rangle, \quad (26)$$

where $\text{FLIP}(j; p, q)$ denotes a binary string obtained from flipping the p th and q th bits of the binary representation of j , and $d_{j,p,q}$ is an integer to be described below.

We will refer to the factor $(-1)^{d_{j,p,q}}$ as the phase factor below. To see where this phase factor comes from, let us examine a simple example in which a one-body operator $a_2^\dagger a_0$ is applied to the state $|j\rangle = |110\rangle$. Using the alternative representation $|j\rangle = |110\rangle = a_0^\dagger a_1^\dagger |vac\rangle$, we obtain

$$a_2^\dagger a_0 |110\rangle = a_2^\dagger a_0 a_0^\dagger a_1^\dagger |vac\rangle = a_2^\dagger a_1^\dagger |vac\rangle = -|011\rangle. \quad (27)$$

However, the right-hand side of Eq. (27) is not a valid basis state because the subscripts of the creation operators are not in increasing order. It follows from Eq. (25) that we can rearrange the creation operators by using the anti-commutation identity, which introduces a negative sign. As a result, we obtain

$$a_2^\dagger a_0 |110\rangle = -|011\rangle. \quad (28)$$

For a general one-body interaction term, the phase factor resulting from applying $a_p^\dagger a_q$ to $|j\rangle \equiv |j_0 j_1 \dots j_{n-1}\rangle$, with assumption that $p < q$, $|j\rangle_p = |0\rangle$ and $|j\rangle_q = |1\rangle$, can be derived as follows,

$$\begin{aligned} & a_p^\dagger a_q a_{f_0}^\dagger a_{f_1}^\dagger \dots a_q^\dagger \dots a_{f_{n-1}}^\dagger |vac\rangle \\ &= (-1)^{j_0+j_1\dots+j_{q-1}} a_p^\dagger a_{f_0}^\dagger a_{f_1}^\dagger \dots a_q a_q^\dagger \dots a_{f_{n-1}}^\dagger |vac\rangle \\ &= (-1)^{j_0+j_1\dots+j_{q-1}} a_p^\dagger a_{f_0}^\dagger a_{f_1}^\dagger \dots [1 - a_q^\dagger a_q] \dots a_{f_{n-1}}^\dagger |vac\rangle \\ &= (-1)^{j_0+j_1\dots+j_{q-1}} a_p^\dagger a_{f_0}^\dagger a_{f_1}^\dagger \dots \times 1 \times \dots a_{f_{n-1}}^\dagger |vac\rangle \\ &= (-1)^{j_{p+1}+j_{p+2}\dots+j_{q-1}} a_{f_0}^\dagger a_{f_1}^\dagger \dots a_p^\dagger \dots a_{f_{n-1}}^\dagger |vac\rangle. \end{aligned} \quad (29)$$

In the first step of the derivation, we move a_q to the right using the anti-commutation identity Eq. (22) until it is just to the left of a_q^\dagger . Each time the anti-commutation identity is invoked, we pick up a negative sign. The total number of negative signs we pick up is the number of creation operators to the left of a_q^\dagger . This number is the same as the number of 1's in the binary representation of j , i.e., $j_0 j_1 \dots j_{q-1} j_q \dots j_{n-1}$, to the left of the q th bit, which is identical to $j_0 + j_1 + \dots + j_{q-1}$.

We then replace $a_q a_q^\dagger$ with $1 - a_q^\dagger a_q$ using the the anti-commutation identity in Eq. (21). This effectively splits $a_p^\dagger a_q |j\rangle$ into two terms. The second term vanishes because applying a_q to a basis state in which the q th single particle state is unoccupied results in 0. In the next step, we again use the anti-commutation identity in Eq. (22) to move a_p to the right place in the ordered integer sequence $f_0, f_1, \dots, p, \dots, f_{n-1}$. Such movements produce a multiplicative factor $(-1)^{j_0+j_1+\dots+j_{p-1}}$. Combining it with the multiplicative factor $(-1)^{j_{p+1}+j_{p+2}\dots+j_{q-1}}$ produced from the first step of the derivation, we obtain the final phase factor

$$\begin{aligned} (-1)^{d_{j,p,q}} &= (-1)^{j_0+\dots+j_{p-1}} \times (-1)^{j_0+\dots+j_{p-1}+j_p+\dots+j_{q-1}} \\ &= (-1)^{j_{p+1}+j_{p+2}\dots+j_{q-1}}. \end{aligned} \quad (30)$$

The derivation of such phase factor only relies on the fact that $p \neq q$. The expression of phase factor $d_{j,p,q}$ is similar for $p > q$,

$$\begin{aligned} (-1)^{d_{j,p,q}} &= (-1)^{j_0+\dots+j_{q-1}} \times (-1)^{j_0+\dots+j_{q-1}+0+j_{q+1}+\dots+j_{p-1}} \\ &= (-1)^{j_{q+1}+j_{q+2}\dots+j_{p-1}}. \end{aligned} \quad (31)$$

The derivation is similar except for the phase factor generated by a_p^\dagger . Instead of $(-1)^{j_0+\dots+j_{p-1}}$, the j_q in the phase factor should be replaced by zero as a_q has been applied to $|j\rangle$. In the special case when $p = q$ or $|p - q| = 1$, it can be seen that the phase factor equals to 1 or equivalently $d_{j,p,q} = 0$.

For a general two-body interaction term, the phase factor resulting from applying $a_p^\dagger a_q^\dagger a_r a_s$ to $|j\rangle \equiv |j_0 j_1 \dots j_{n-1}\rangle$ can be derived similarly. Clearly, not all combinations of $a_p^\dagger, a_q^\dagger, a_r, a_s$ contribute to a nonzero matrix element in \mathcal{H} . For example, when $p = q$ or $r = s$, $a_p^\dagger a_q^\dagger a_r a_s |j\rangle = 0$ for all j because we cannot create or annihilate the same state twice.

In general, whether the two-body operator contributes a non-zero matrix element to the j th column of \mathcal{H} depends on the value of p, q, r and s as well as the state of the i th qubit in $|j\rangle$ for $i = p, q, r, s$.

When 1) $p = r$ and $q \neq s$, 2) $p = s$ and $q \neq r$, 3) $q = r$ and $p \neq s$ and 4) $q = s$ and $q \neq r$, the corresponding two-body interaction term becomes $a_p^\dagger a_q^\dagger a_p a_s$, $a_p^\dagger a_q^\dagger a_r a_p$, $a_p^\dagger a_q^\dagger a_q a_s$ or $a_p^\dagger a_q^\dagger a_r a_q$ respectively. Using the anticommutation identity, we can rewrite these terms as $-n_p a_q^\dagger a_s$, $n_p a_q^\dagger a_r$, $n_q a_p^\dagger a_s$ and $-a_p^\dagger a_r n_q$ respectively. Because $n_q |j\rangle$ is either 0 or $|j\rangle$, these special instances of the two-body term effectively reduce to one-body terms. In the case $p = r$ and $q = s$, the two-body term simplifies to the product of two number operators $n_p n_q$.

Note that there cannot be three or more identical indices in the creation and annihilation operators contained in a two-body term because, in this case, two creation operators or two annihilation operators will be identical. As we discussed earlier, this type of two-body term yields 0 when it is applied to $|j\rangle$ for any j .

Therefore, it suffices to examine the phase factors produced by the following four types of operators: $n_p a_q^\dagger a_s$ with $q \neq s$, $a_p^\dagger a_r n_q$ with $p \neq r$, $n_p n_q$ and $a_p^\dagger a_q^\dagger a_r a_s$ with distinct p, q, r, s . The first two cases reduce to the one-body case discussed earlier in which the phase factor is defined by Eq. (30) or Eq. (31). The third case does not introduce a phase factor at all.

For the last case in which p, q, r, s are all different, we assume, without loss of generality, that $p < q$ and $r > s$. In this case, applying the two-body operator to $|j\rangle$ yields a different basis state if $|j\rangle_p = |0\rangle$, $|j\rangle_q = |0\rangle$, $|j\rangle_r = |j\rangle$ and $|j\rangle_s = |j\rangle$. The phase factor resulting from operation can be derived in two steps. In the first step, we examine the phase factor resulting from applying $a_r a_s$ to $|j\rangle$. It can be easily verified that such a phase factor is in fact

$$(-1)^{d_{j,r,s}} = (-1)^{j_{s+1} + \dots + j_{r-1}}. \quad (32)$$

The product of this phase factor and the state

$$|j'\rangle = |\text{FLIP}(j; r, s)\rangle \quad (33)$$

is the outcome of $a_r a_s |j\rangle$.

In the second step, we derive the phase factor associated with applying $a_p^\dagger a_q^\dagger$ to $|j'\rangle$ defined by Eq. (33). It can be easily shown that such a factor is

$$(-1)^{d_{j',p,q}} = (-1)^{j'_{p+1} + \dots + j'_{q-1}}. \quad (34)$$

As a result, the total phase factor associated with applying the two-body operator $a_p^\dagger a_q^\dagger a_r a_s$ to $|j\rangle$ is

$$(-1)^{d_{j',p,q} + d_{j,r,s}}. \quad (35)$$

The resulting state is

$$a_p^\dagger a_q^\dagger a_r a_s |j\rangle = (-1)^{d_{j',p,q} + d_{j,r,s}} |\text{FLIP}(\text{FLIP}(j; r, s); p, q)\rangle. \quad (36)$$

C. Oracle construction

In this subsection, we detail the O_C oracle (SPARSITY oracle) within our formalism for one-body and two-body interactions. By constructing a few examples of interactions, we demonstrate how the framework can be generalized. While the efficient construction of the O_C oracle varies slightly for different types of Hamiltonians, these differences are minor. We will discuss the construction of the O_C oracle separately for each type of interaction.

1. One-body interactions

To begin, we consider a one-body Hamiltonian given by:

$$\mathcal{H} = \sum_{p \neq q} a_p^\dagger a_q. \quad (37)$$

The O_C oracle O_c can be constructed as a combination of two oracles: the O_s oracle and the O_ϕ oracle. The O_s oracle is defined as:

$$\begin{aligned} O_s |1\rangle |p\rangle |q\rangle |j\rangle \\ = \begin{cases} |0\rangle |p\rangle |q\rangle |\text{FLIP}(j, p, q)\rangle & \text{if } |j\rangle_p = 0 \text{ and } |j\rangle_q = 1, \\ |1\rangle |p\rangle |q\rangle |j\rangle & \text{otherwise.} \end{cases} \end{aligned} \quad (38)$$

The O_ϕ oracle can be defined as

$$O_\phi |p\rangle |q\rangle |j\rangle = (-1)^{d_{j,p,q}} |p\rangle |q\rangle |j\rangle. \quad (39)$$

Define SPARSITY oracle O_c as

$$O_c := O_s O_\phi. \quad (40)$$

Consider the action of O_c on a state $|j\rangle$,

$$\begin{aligned} O_c |1\rangle |p\rangle |q\rangle |j\rangle \\ = O_s O_\phi |1\rangle |p\rangle |q\rangle |j\rangle \\ = (-1)^{d_{j,p,q}} O_s |1\rangle |p\rangle |q\rangle |j\rangle \\ = (-1)^{d_{j,p,q}} |o(j, p, q)\rangle |p\rangle |q\rangle |\text{FLIP}(j, p, q)\rangle, \end{aligned} \quad (41)$$

where

$$|o(j, p, q)\rangle = \begin{cases} |0\rangle & \text{if } |j\rangle_p = 0 \text{ and } |j\rangle_q = 1, \\ |1\rangle & \text{otherwise.} \end{cases} \quad (42)$$

For a fixed (p, q) pair, the corresponding phase oracle O_ϕ can be constructed using the circuit shown on the right-hand side of the equation in Fig. 4. Each Z gate in the circuit accounts for the $(-1)^{j_k}$ factor in Eq. (30) for $k = p+1, \dots, q-1$. To construct the phase oracle for the sum $\sum_{p,q} a_p^\dagger q_q$, controls can be placed on the qubits representing $|p\rangle$ and $|q\rangle$ to select the appropriate circuit for each one-body term. This approach, as outlined in [24], requires $\mathcal{O}(n^2)$ circuit blocks and at least $\mathcal{O}(n^2)$ gates.

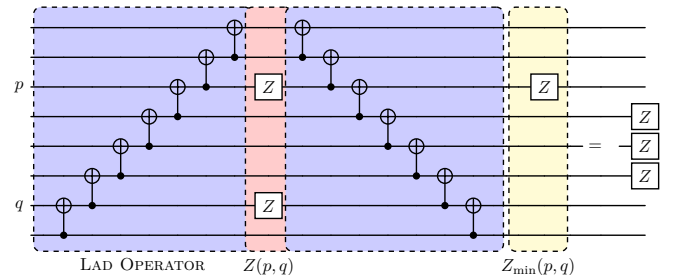


FIG. 4: Illustration of a circuit identity for the construction of O_ϕ . Note that in the circuit, the two Pauli Z gates are placed on the p -th and q -th gate where $p < q$.

Using previously developed techniques [2, 37], the number of circuit blocks and gates can be significantly reduced. One of the key things to observe is that the

circuit on the right hand side of the equation in Fig. 4 is equivalent to the circuit on the left hand side which consists of a set of staggered CNOTs starting from the least significant qubit and ending at the most significant qubit used to encode $|j\rangle$. We refer to this set of staggered CNOTs as a ladder circuit. The ladder circuit is followed by two Z gates placed on the p -th and q -th qubits respectively. The inverse of the ladder operator is then applied to undo the ladder operation. Readers are referred to [37] for verification that the equation in Fig. 4 holds.

At first glance, the circuit on the left-hand side of the equation in Fig. 4 may appear to use more gates than the circuit on the right. However, when combined with a circuit that performs the so-called “SWAP-UP” operation, which moves the state of a specific qubit in the register encoding $|j\rangle$ to the first (least significant) qubit of this register, the operation on the right-hand side of Fig. 4 can be performed simultaneously for all combinations of p and q .

Formally, the SWAP-UP (denoted by $SW(p)$ below) is defined as [43]

$$SW(p) : |p\rangle |j_0\rangle |j_1\rangle \cdots |j_{n-1}\rangle \rightarrow |p\rangle |j_p\rangle |*\rangle \cdots |*\rangle. \quad (43)$$

Note that the operation can be generalized such that j_i is of length m_b . The SWAP-UP operation requires $m_b n + \lceil \log_2(n) \rceil$ qubits, and $8m_b n + \mathcal{O}(\log(n))$ T gate count with $\log(n)$ T depth.

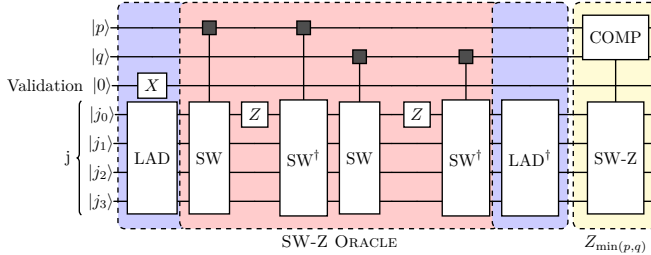


FIG. 5: Illustration of quantum circuit for O_ϕ for one-body interaction $a_p^\dagger a_q, a_p a_q, a_p^\dagger a_q^\dagger$ when $p \neq q$.

It is not difficult to verify that the circuit block in the shaded region of Fig. 5, which implements $SW(p)(Z \otimes I)SW^\dagger(p)$ effectively places a Z gate on the p -th qubit of the target register that encodes $|j\rangle$. Similarly, $SW(q)(Z \otimes I)SW^\dagger(q)$ places a Z gate on the q -th qubit of the target register. We refer to the circuit block that excludes the controlling qubits at the top of the circuit (for encoding p and q) as a SW-Z block. Note that this block is identical in $SW(p)$ and $SW(q)$.

By using Hadamard gates applied to $|0\rangle$ to generate a superposition of $|p\rangle$ and $|q\rangle$, we can effectively generate a superposition of $SW(q) \cdot SW(p)$ circuits that apply appropriate phase factors associated with different $a_p^\dagger a_q$ terms.

The last gate involves the COMP and SW-Z gate. The COMP oracle, designed in [55], compares the $|p\rangle$ and $|q\rangle$. Based on the output from COMP, SW-Z gate can

impose $Z_{\min(p,q)}$ in the circuit. We emphasize that the O_ϕ constructed here mainly works for the case $p \neq q$ but can be easily extended for $p = q$ as well by adding additional control on $p = q$.

The O_s oracle is based on a similar approach to the O_C oracle introduced in [24]. We use the SW gate to reduce the complexity of looking up the classical data stored in p -th qubit, illustrated in Fig. 6a. The first ancilla qubit is used to mark whether the computation is valid or not. Its value is initially set to be $|1\rangle$. Through checking the $|j\rangle_p$ and $|j\rangle_q$ by SW gate and recording them in two ancilla qubits, we can make the computation valid if $|j\rangle$ satisfies that $|j\rangle_p = 0$ and $|j\rangle_q = 1$. Based on whether the computation is valid or not (the control from the first ancilla qubit), we use the SW gate to swap up the p -th qubit and apply a NOT gate. The same process has been done to the q -th qubit, and an additional CNOT gate is applied to uncompute the classical data stored on the third qubit.

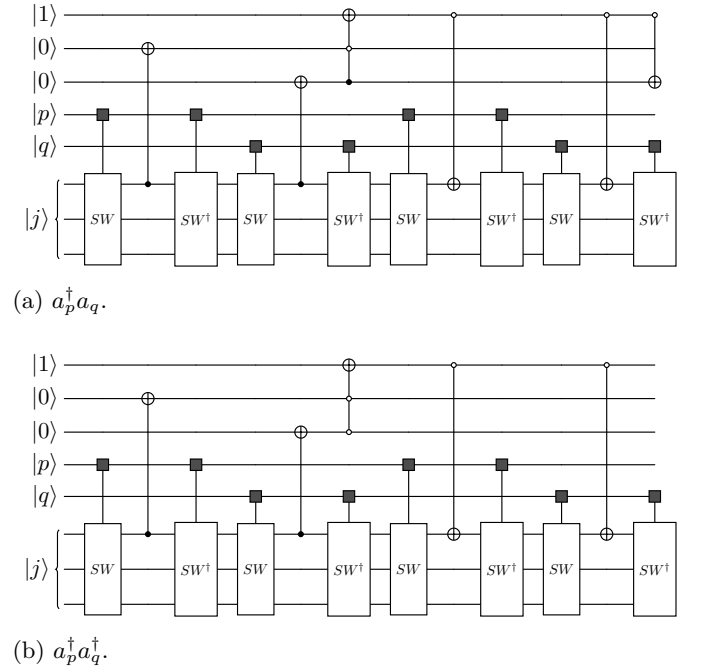


FIG. 6: Illustrations of the O_s oracle for one-body interactions, where SW denotes the SWAP-UP gate used in [3, 43].

To estimate the cost of the phase oracle O_ϕ , we employ two ladder oracles (LAD), each requiring n CNOT gates, and apply the SWAP-UP operation twice to implement Z_p on the input state. For the O_s oracle, a total of eight SWAP-UP operations are used, as illustrated in Figs. 6a and 6b. Consequently, for the one-body interaction, the O_C oracle has a T-gate count of $\mathcal{O}(n)$ and a T-depth of $\mathcal{O}(\log n)$, following the resource estimates in [3, 43].

2. Number operator

We consider a Hamiltonian

$$\mathcal{H} = \sum_p a_p^\dagger a_p, \quad (44)$$

and discuss the construction of the O_C oracle for this Hamiltonian. Specifically, the goal is to design two oracles, O_s and O_ϕ . For number operators, no non-trivial phase is generated, and O_ϕ acts as the identity operator. Therefore, it suffices to construct the O_s oracle,

$$O_s |1\rangle |p\rangle |j\rangle = \begin{cases} |0\rangle |p\rangle |j\rangle & \text{if } |j\rangle_p = 1, \\ |1\rangle |p\rangle |j\rangle & \text{otherwise.} \end{cases} \quad (45)$$

For number operators, no non-trivial phase is generated, and O_ϕ acts as the identity operator. Therefore, it suffices to construct the O_s oracle. Using the SW gate, we can determine whether $|j\rangle_p$ equals $|0\rangle$ or $|1\rangle$. Fig. 7 illustrates the construction of the O_C oracle, maintaining a structure comparable to Fig. 5 to highlight that the phase is always 1 for number operators.

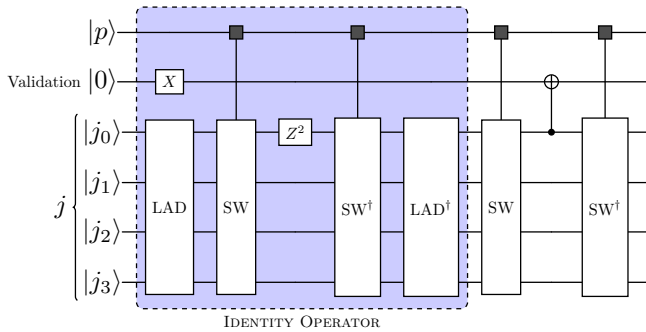


FIG. 7: Illustration of the O_C oracle for a Hamiltonian expressed as a summation of number operators. It is worth noting that the first part of the circuit, located between the two LAD oracles, is equivalent to an identity operation where $Z^2 = Z \cdot Z = I$. This structure is used to facilitate comparison with the O_C oracle for general one-body interactions.

We have discussed the O_C oracle for both cases, $p = q$ and $p \neq q$. By incorporating an additional control to distinguish whether $p = q$, we can construct an O_C oracle for general one-body interactions, as illustrated in Fig. 8.

3. Two-body interactions

In this section, we discuss the O_C oracle for two-body interactions. Before delving into the details, it is important to note that the O_C oracle described here has only minor variations across different types of interactions, including $a_p^\dagger a_q^\dagger a_r a_s$, $n_p n_q$ and $n_r a_p^\dagger a_q$. By block encoding each type of interaction, LCU techniques can ultimately

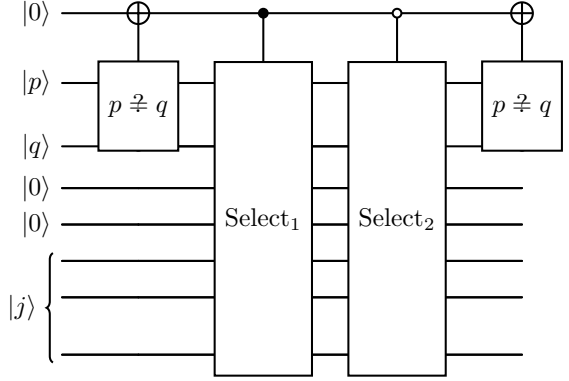


FIG. 8: Illustration of O_C oracle for one-body interaction $a_p^\dagger a_q$. We use Select₁ and Select₂ to denote the different O_C oracles designed in Fig. 5 and Fig. 7. The gate marked with $p \neq q$ serves as the control for the NOT gate: the NOT gate is applied only when $p = q$.

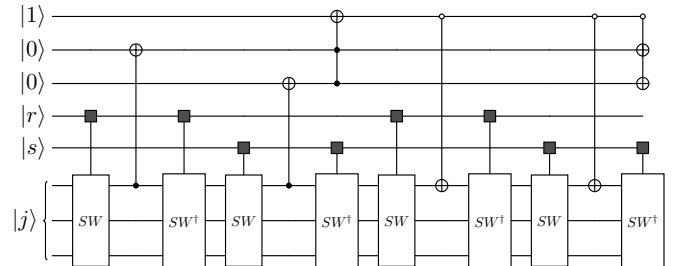


FIG. 9: Illustration of O_s oracle for one-body interaction $a_r a_s$ where SW is used to denote the SWAP-UP gate used in [3, 43].

be applied to provide the input model for the full Hamiltonian.

For the two-body interaction, there are three distinct types. The first type of interaction is given by:

$$a_p^\dagger a_q^\dagger a_r a_s, \quad (46)$$

where $p < q$ and $r > s$. For simplicity, we initially assume that p , q , r , and s are four distinct indices. The general form can be extended by adding controls to handle cases where $p = q$ or $r = s$. Notably, the O_C oracle is only required to function for the specific ordering of p , q , r , and s , as the O_C oracle can be set to assign zero coefficients to all other orderings. We aim to design a SPARSITY oracle O_c such that

$$\begin{aligned} O_c |1\rangle |1\rangle |p\rangle |q\rangle |r\rangle |s\rangle |j\rangle \\ = (-1)^{d_{j',p,q} + d_{j,r,s}} |o_1(j, p, q)\rangle |o_2(j, r, s)\rangle \\ \times |\text{FLIP}(j'; r, s)\rangle, \end{aligned} \quad (47)$$

where $j' = |\text{FLIP}(j; p, q)\rangle$. The o_1 and o_2 indicate whether $a_p^\dagger a_q^\dagger$ and $a_r a_s$ are valid computation for the

state $|j\rangle$. To be specific,

$$|o_1(j, p, q)\rangle = \begin{cases} |0\rangle & \text{if } |j\rangle_p = 0 \text{ and } |j\rangle_q = 0, \\ |1\rangle & \text{otherwise,} \end{cases} \quad (48)$$

and

$$|o_2(j, r, s)\rangle = \begin{cases} |0\rangle & \text{if } |j\rangle_r = 1 \text{ and } |j\rangle_s = 1, \\ |1\rangle & \text{otherwise.} \end{cases} \quad (49)$$

The design of such an O_C oracle is derived directly from the O_C oracle for the two one-body operators $a_p^\dagger a_q^\dagger$ and $a_r a_s$. The O_s oracles for these two types of interactions are shown in Fig. 6b and Fig. 9. The phase oracle for both operators is identical to the one illustrated in Fig. 5. By stacking these two O_C oracle together, the desired O_C oracle is obtained, as illustrated in Fig. 10. To account for cases where $p = q$ or $r = s$, the same procedure as in Fig. 8 is applied.

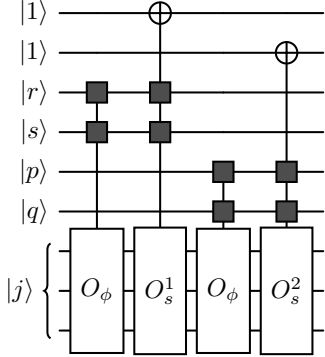


FIG. 10: Illustration of O_C oracle for two-body interaction $a_p^\dagger a_q^\dagger a_r a_s$ where SW is used to denote the SWAP-UP gate used in [3, 43]. The O_s^1 and O_s^2 are part of O_C oracle designed for $a_p^\dagger a_q^\dagger$ and $a_r a_s$ respectively. We note that we abuse the notation O_ϕ , O_s^1 and O_s^2 in the circuit illustration as we do not include the control on p, q, r, s as well as validation qubits in the two oracle, aiming to clarify the structure of circuit better.

The O_C oracle for two-body interaction can be designed with less cost if the interaction has special structures, for example,

$$n_p n_q \text{ or } n_r a_p^\dagger a_q. \quad (50)$$

To construct the O_C oracle for these interactions, the O_C oracle (including O_ϕ and O_s) for $a_p^\dagger a_q^\dagger$ and $a_r a_s$ is replaced with an O_C oracle for $a_p^\dagger a_q$ and the number operator n . This process is illustrated in Fig. 5 and Fig. 7. We note that additional control of $p = q$ is needed for the O_C oracle to include the designs for the O_C oracle in both the case of $p = q$ and $p \neq q$, as illustrated in Fig. 8 and Fig. 11.

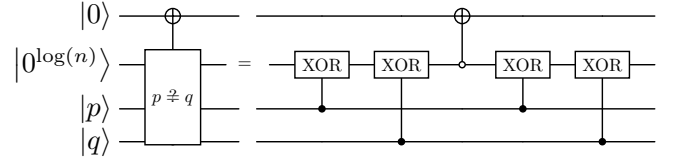


FIG. 11: Illustration of implementation of condition $p = q$ in O_C oracle constructed in Fig. 8. If $p = q$, the first qubit is in state $|0\rangle$; otherwise it is in state $|1\rangle$.

4. Beyond two-body interaction

The generalization of the O_C oracle to three-body interactions and beyond follows a similar approach to the O_C oracles for one-body and two-body interactions. The additional cost primarily arises from the increased use of SWAP circuits [43]. It is also worth noting that the O_C oracle can be extended to handle Hamiltonians that do not conserve particle number. However, the specific details of the circuit design for such Hamiltonians are beyond the scope of this paper and are left for future work.

V. AMPLITUDE ORACLE O_A

In previous work [24–26], the O_A oracle, which encodes numerical values of all matrix elements of the Hamiltonian, is composed of a sequence of controlled rotations with the rotation angle determined by the values of the coefficients h_{ijkl} in Eq. (20).

The number of controlled rotations is the number of terms in one and two-body operators which is in general n^2 and n^4 . It would be desirable to reduce the number of controlled gates in a block encoding circuit. This can be done using a table lookup input model described below.

Another potential problem with using controlled rotation is that the unitary

$$R(\theta) = \begin{bmatrix} \cos(\theta) & \sin(\theta) \\ -\sin(\theta) & \cos(\theta) \end{bmatrix} \quad (51)$$

required to perform the rotation may not be a native gate, therefore may need to be decomposed further into products of other simpler unitaries to yield an approximate rotation.

The data lookup input model, which makes use of a previously developed SELECT-SWAP circuit, provides an efficient mechanism to encode the coefficients as probability amplitudes of a superposition state.

To simplify the discussion, we assume that the Hamiltonian to be block-encoded contains L distinct coefficients corresponding to the one-body and two-body terms. Note that the notation L is slightly abused, as this number may be smaller than the total number of terms in certain structured Hamiltonians in Sec. VIII B.

The coefficient of each term is ρ_l for $l = 0, 1, \dots, L - 1$.

$$\frac{1}{L} \sum_{l \in [L]} |0^{m_b-1}\rangle (\rho_l |0\rangle + (\text{sgn}(\rho_l) - \rho_l) |1\rangle) |l\rangle + *, \quad (52)$$

where $\text{sgn}(x) = -1$ if $x < 0$, and $\text{sgn}(x) = 1$ otherwise, when it is applied to the superposition state $\frac{1}{\sqrt{L}} \sum_{l \in [L]} |0\rangle |l\rangle$, produced by applying $I \otimes D_s$ to $|0\rangle |0^m\rangle$ where $m = \log(L)$ and D_s is a Kronecker products of Haddamard matrices. The number of the leading ancilla qubits m_b in Eq. (52) is determined determined by the accuracy of the block encoding and is discussed further in Sec. V B. Also, $*$ denotes those states that are excluded upon post-selecting the state $|0^{m_b}\rangle$ in the first quantum register, which consists of m_b qubits.

This circuit is constructed in two steps. In the first step, we construct an efficient circuit O_B as a data-lookup oracle that can map l to a binary representation of a finite precision approximation of ρ_l which we denote by b_l , i.e.,

$$O_B : |l\rangle |0^{m_b}\rangle \rightarrow |l\rangle |b_l\rangle. \quad (53)$$

In the second step, we construct a *sampling* circuit O_S that can turn $|b_l\rangle$ into an amplitude factor $|0\rangle |l\rangle$, i.e.,

$$\begin{aligned} O_S : & |b_l\rangle |0^{m_b-1}\rangle |0\rangle \\ & \rightarrow |b_l\rangle |0^{m_b-1}\rangle (\rho_l |0\rangle + (\text{sgn}(\rho_l) - \rho_l) |1\rangle) + *. \end{aligned} \quad (54)$$

We apply another O_B oracle to uncompute $|b_l\rangle$.

A. Data-lookup oracle

A m_b -bit binary representation of a finite precision approximation to the coefficient ρ_l can be generated by applying a sequence of X gate to turn some of the qubits in $|0^{m_b}\rangle$ from $|0\rangle$ to $|1\rangle$ to yield $|b_l\rangle$. We will use $X^{b_l} |0^{m_b}\rangle$ to represent such an operation. A superposition of $X^{b_l} |0\rangle$ can be generated using a selection circuit shown in Fig. 13. The application of X^{b_l} is activated by an single $|l\rangle$ -controlled NOT that turns a controlling ancilla qubit from $|0\rangle$ to $|1\rangle$. The activated controlling qubit is reset to $|0\rangle$ once X^{b_l} is applied to $|0^{m_b}\rangle$. In this case, the number of T gates required to implement multi-qubit CNOT gates is $\mathcal{O}(L)$.

It is not efficient to implement every X^{b_l} with a multi-qubit control. The SELECT-SWAP technique uses $\mathcal{O}(\log(\frac{L}{\lambda}))$ sets of ancilla qubits to group all $X^{b_l} |0^{m_b}\rangle$ operations into $\mathcal{O}(\frac{L}{\lambda})$ groups as shown in Fig. 13a where $L = 16$, $\lambda = 4$ and $m_b = 1$. The circuit for general m_b is illustrated in Fig. 12 where the select part is not included as it is same as the original $m_b = 1$ version, except that more CNOT gates are needed.

We seek to construct a circuit for O_A oracle that yields

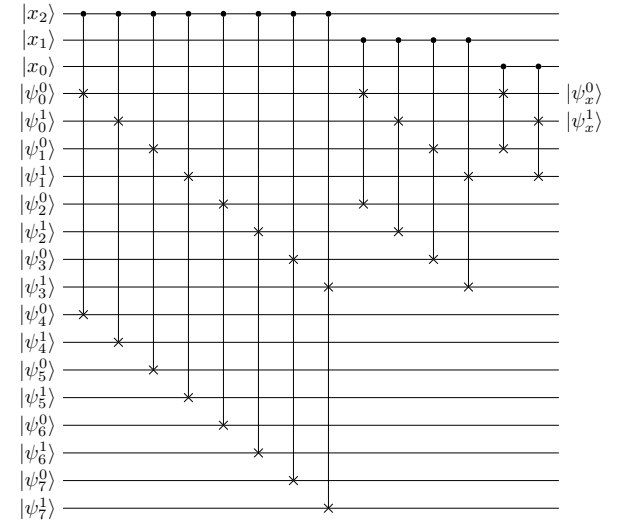


FIG. 12: A multi-qubit extension of the single qubit swap in Ref. [37]

We skip the discussion of compilation of the SELECT-SWAP circuit (see [43] for a comprehensive resource estimate) and only summarize the overall cost for the SELECT-SWAP circuit. In total, the oracle requires

$$\lambda m_b + 2\lceil \log_2(L) \rceil \quad (55)$$

qubits,

$$4 \left\lceil \frac{L}{\lambda} \right\rceil + 8\lambda m_b \quad (56)$$

T gates and generating a circuit that has a T-depth of

$$\frac{L}{\lambda} + \log(\lambda). \quad (57)$$

The λ can be interpreted as the number of classical data within each group. From the cost, it can be observed that we are able to minimize total T gate count by tuning the parameter λ . When $\lambda = \sqrt{\frac{L}{m_b}}$, we can obtain the optimal T gate complexity of $\mathcal{O}(\sqrt{Lm_b})$.

The majority of Clifford gates within SELECT-SWAP could come from control multi-NOT gates, used for loading classical data. For a quantum device with all-to-all connectivity, one way to implement such a gate is by using $Lm_b + o(L)$ CNOT gates with a circuit depth of the same scaling. However, we note that with mid-circuit measurement and qubit reset, every quantum circuit in the Clifford group can be performed with $\mathcal{O}(1)$ depth with measurement-based quantum computation (MBQC) [56, 57] and similar Clifford gate cost. Such a measurement-based approach can also achieve constant depth, even when the hardware lacks all-to-all connectivity [58].

The SELECT-SWAP circuit is a framework for a quantum data lookup input model that encodes classical data on a quantum device. It is not necessary to optimize toward lowering the T gate count. Indeed, the previously developed PREPARE oracle in [1] employs QROM, which can be regarded as using a SELECT-SWAP circuit with $\lambda = 1$, i.e., optimizes qubit usage but incurs a linear T gate count. A comprehensive review of different data lookup schemes within a unified architecture is presented in Ref. [59], which also demonstrates how SELECT-SWAP can be tuned for 2D local connectivity of qubits, exhibiting noise resilience while achieving sub-linear scaling across all resource measures.

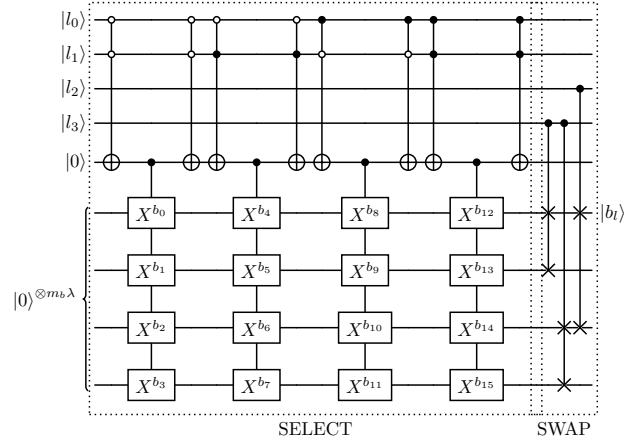
B. Direct sampling method

To prepare a desired quantum state, an additional oracle is required to convert the binary representation of a coefficient into probability amplitude. For a binary string b with first bit b_0 representing sign of the number it represents and last $m_b - 1$ bits (denoted by b_1) representing a real number $0 \leq r_b \leq 1$, a sampling oracle is constructed to map $|b\rangle |0^{m_b-1}\rangle |0\rangle$ to

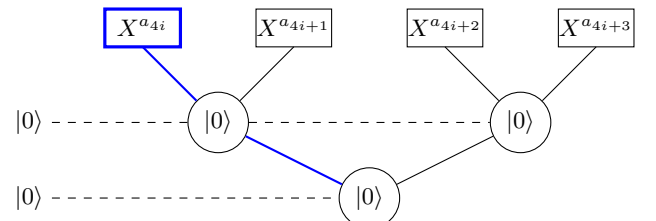
$$|b\rangle |0^{m_b-1}\rangle (r_b |0\rangle + (\text{sgn}(r_b) - r_b) |1\rangle) + *, \quad (58)$$

where $*$ is used to indicate the dropped states after post-selection on the state $|0^{m_b}\rangle$.

When the number of coefficients L in the Hamiltonian greatly exceeds the ℓ_1 norm of the coefficients (for instance, for two-body interactions, the ℓ_1 norm of the coefficients h_{pqrs} is defined as $\sum_{p,q,r,s=0}^{n-1} |h_{pqrs}|$), alias sampling [1] has been proposed to reduce the subnormalization factor from L to the ℓ_1 norm of the coefficients. However, this is unnecessary if each coefficient is $\mathcal{O}(1)$ or if the coefficients are known to decrease with respect to their indices (or index differences). In such cases, a direct sampling approach to be presented below reduces



(a) The SELECT-SWAP circuit introduced in Ref. [43], for word length $m_b = 1$, tuning parameter $\lambda = 4$, and $L = 16$. If the stored bit at address a_i is 0, then X^{a_i} is the identity; otherwise, it is a Pauli X . The upper half of the address bits is used by the SELECT subcircuit to pick the column of X^{a_i} , and the SWAP subcircuit uses the lower half to extract the row. The classical bit is then routed to $|a_x\rangle$. The optimal version is given in Ref. [43, Fig. 1(d)].



(b) High-level routing scheme of the SWAP subcircuit for $N = 16$. The index $i \in \{0, 1, 2, 3\}$ represents the column activated by the SELECT subcircuit. The controlled-SWAPs (circles) act as a router, carving a path (blue) through the binary tree to retrieve the classical bit.

FIG. 13: SELECT-SWAP circuit and its routing scheme through the binary tree.

the additional subnormalization introduced by diffusion operators.

The construction of the sampling circuit is illustrated in Fig. 14. Initially, $|0\rangle^{m_b-1}$ is diffused to produce the superposition

$$\sum_i^{2^{m_b-1}-1} \frac{1}{\sqrt{2^{m_b-1}}} \underbrace{|b_0\rangle |b_1\rangle}_{|b\rangle} |i\rangle |0\rangle. \quad (59)$$

Next, $|b_1\rangle$ and $|i\rangle$ are compared using a comparison oracle [60]. If $b_1 > i$, the last qubit is flipped, resulting

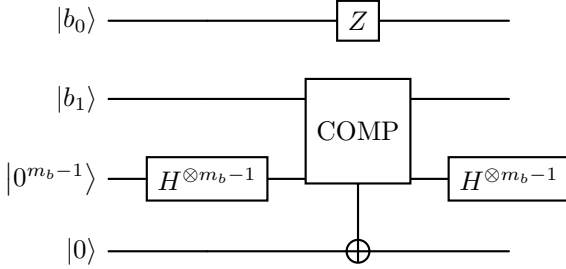


FIG. 14: Illustration of sampling approach to transform classical data from data-lookup into the coefficient factors.

in:

$$\begin{aligned} & \frac{1}{\sqrt{2^{m_b-1}}} \sum_{i=0}^{b_1-1} |b_0\rangle |b_1\rangle |i\rangle |0\rangle \\ & + \frac{1}{\sqrt{2^{m_b-1}}} \sum_{i=b_1}^{2^{m_b-1}-1} |b_0\rangle |b_1\rangle |i\rangle |1\rangle. \end{aligned} \quad (60)$$

We apply another $m_b - 1$ Hadamard gates on $m_b - 1$ qubits after the state $|b_0\rangle |b_1\rangle$ and Z gate on $|b_0\rangle$. Therefore, we have that

$$|b\rangle |0^{m_b-1}\rangle (r_b |0\rangle + (\text{sgn}(r_b) - r_b) |1\rangle) + |b\rangle |\Psi\rangle, \quad (61)$$

where $|\Psi\rangle$ is used to indicate the dropped states after post-selection for the first $m_b - 1$ qubits on the state $|0^{m_b-1}\rangle$. The $r_b = (-1)^{b_0} \cdot \frac{b_1}{2^{m_b-1}}$ and $m_b - 1$ scales as $\mathcal{O}(\text{polylog}(\frac{1}{\epsilon}))$ for input model with at most ϵ error. The actual format of polynomial dependence relies on the structure of the coefficients tensor in the second-quantized Hamiltonian. The cost of direct sampling coming from $2m_b - 2$ Hadamard gates and one compare oracle. A single call of compare oracle requires $\mathcal{O}(m_b)$ T gate count and generates a circuit of $\mathcal{O}(m_b)$ T gate depth.

C. Oracle construction

There are three main steps in constructing the amplitude oracle using the data-lookup oracle and direct sampling, illustrated in the O_A part within Fig. 15. First, the classical data is loaded via a data-lookup oracle. Next, the direct sampling oracle maps the binary representation of the coefficient to an amplitude in an auxiliary register. Finally, the data-lookup oracle is applied again to uncompute the classical data loaded in the first step.

For data lookup based methods, sampling techniques are required to convert the binary representation of coefficients into their actual coefficient values. For example, alias sampling [48] mentioned earlier has been employed with QROM to prepare quantum states with reduced subnormalization factor [1].

VI. THE COMPLETE CIRCUIT FOR GENERAL HAMILTONIANS

In this section, we show how the circuit gadgets developed for both the SPARSITY oracle O_C and AMPLITUDE oracle O_A in previous sections are assembled together according to the general block encoding circuit diagram shown in Fig. 2. In particular, we specify the additional ancilla qubits required in such a circuit and give an estimation of the gate resources required to implement such a circuit. To simplify our discussion, we continue to use the Hamiltonian defined in Eq. (37) which contains only one-body interactions. The extension of a more general Hamiltonian consisting of both one and two-body interactions is relatively straightforward.

The overall structure of the block encoding circuit for \mathcal{H} is shown in Fig. 15. The O_A and O_C components of the circuit are shaded in red and blue, respectively. Except for the qubits labeled $|j\rangle$ at the bottom of the circuit, all other qubits are ancilla. The first qubit that takes the input of $|0\rangle$ is used to distinguish one-body terms with $p = q$, which is a number operator, and $p \neq q$ using the circuit gadget shown in Fig. 11. The O_C oracles required for these two cases are slightly different. They are implemented by the O_C^1 and O_C^2 circuit blocks shown towards the end of the circuit. Only one of them is activated depending on the outcome of the comparison between p and q , which are generated from the diffusion operator (Hadamard gates) applied to the two sets of qubits that take $|0^{\log(n)}\rangle$ as the input.

A few set of ancilla qubits are used as the input to the O_A oracle. The qubit that takes $|0\rangle$ as the input and the qubits that take the first $|0^{m_b-1}\rangle$ as the input are used for SELECT-SWAP based data lookup circuit (O_B^1 or O_B^2) shown in Fig. 13a. We note that within Fig. 15, there are $m_b \lambda$ ancilla qubits used for the data-lookup circuit but not included within the circuit. These qubits are used to construct data-lookup circuit shown in Fig. 13a. We copy the inquired data, for example b_l , to these m_b qubits illustrated in the Fig. 15. The next set of qubits that take the second $|0^{m_b-1}\rangle$ as the input and the following qubit that takes $|0\rangle$ as the input are used in the direct sampling oracle designed to encode a finite precision approximation to h_{pq} for the corresponding p and q generated from the diffusion operator applied to $|0^{\log(n)}\rangle$ at the beginning of the circuit. The integer m_b is chosen to limit the approximation error of the block encoding circuit to ϵ , which implies the approximation error allowed for each h_{pq} is limited to $\frac{\epsilon}{n^2}$. As a result, the number of qubits required to represent h_{pq} at this accuracy level is on the order of $\mathcal{O}(\log(\frac{n^2}{\epsilon}))$. When block encoding a second-quantized Hamiltonian with two- or three-body interactions, the value of m_b can be determined analogously. If there are L monomials of creation and annihilation operators within the Hamiltonian \mathcal{H} , the m_b should be of complexity $\mathcal{O}(\log(\frac{L}{\epsilon}))$.

Note that we again treat the number operator ($p = q$) separately from the case in which $p \neq q$. The leading

Model	Reference	Qubit	Subnormalization factor	T count	T depth
General	Babbush et al. (2018) [1]	$\mathcal{O}(n + \log(\frac{n^4}{\epsilon}))$	$\mathcal{O}(n^4)$	$\mathcal{O}(n^4 + \log(\frac{n^4}{\epsilon}))$	$\mathcal{O}(n^4)$
	This paper	$\mathcal{O}(n + \lambda_1 \log(\frac{n^4}{\epsilon}))$	$\mathcal{O}(n^4)$	$\mathcal{O}(\frac{n^4}{\lambda_1} + \lambda_1 \log(\frac{n^4}{\epsilon}))$	$\mathcal{O}(\frac{n^4}{\lambda_1} + \log \lambda_1)$
Factorized	Kivlichan et al.(2018) [2]	N/A	N/A	$\mathcal{O}(n^2 \log(\frac{1}{\epsilon}))$	$\mathcal{O}(n)$
TI Factorized	Babbush et al.(2018) [1]	$\mathcal{O}(n + \log(\frac{n^2}{\epsilon}))$	$\mathcal{O}(n^2)$	$\mathcal{O}(n + \log(\frac{n^2}{\epsilon}))$	$\mathcal{O}(n)$
	This paper	$\mathcal{O}(n + \lambda_2 \log(\frac{n^2}{\epsilon}))$	$\mathcal{O}(n^2)$	$\mathcal{O}(n + \frac{n}{\lambda_2} + \lambda_2 \log(\frac{n^2}{\epsilon}))$	$\mathcal{O}(\frac{n}{\lambda_2} + \log \lambda_2)$
Localized	Wan (2021) [3]	$\mathcal{O}(n)$	$\mathcal{O}(n^2)$	$\mathcal{O}(n) + \text{PREP}$	$\mathcal{O}(n) + \text{PREP}$
	This paper	$\tilde{\mathcal{O}}(n + \lambda_3 \log(\frac{n^2}{\epsilon}))$	$\mathcal{O}(n^2 \log^2(\frac{n^2}{\epsilon}))$	$\tilde{\mathcal{O}}(\frac{n^2}{\lambda_3} \log^2(\frac{n^2}{\epsilon}) + \lambda_3 \log(\frac{n^2}{\epsilon}))$	$\mathcal{O}(n + \frac{n^2}{\lambda_3} \log^2(\frac{n^2}{\epsilon}) + \log \lambda_3)$

(a) Full Hilbert space (no particle-number constraint).

Model	Reference	Qubit	Subnormalization factor	T count	T depth
General	Babbush et al.(2018) [1]	$\mathcal{O}(n + \log(\frac{n^4}{\epsilon}))$	$\mathcal{O}(n^4)$	$\mathcal{O}(n^4 + \log(\frac{n^4}{\epsilon}))$	$\mathcal{O}(n^4)$
	This paper	$\mathcal{O}(n + \tilde{\lambda}_1 \log(\frac{n^2 \eta^2}{\epsilon}))$	$\mathcal{O}(n^2 \eta^2)$	$\mathcal{O}(n \log \eta + \frac{n^4}{\lambda_1} + \tilde{\lambda}_1 \log(\frac{n^2 \eta^2}{\epsilon}))$	$\mathcal{O}(n \log \eta + \frac{n^4}{\lambda_1} + \log \tilde{\lambda}_1)$
Factorized	Kivlichan et al.(2018) [2]	N/A	N/A	$\mathcal{O}(n^2 \log(\frac{1}{\epsilon}))$	$\mathcal{O}(n)$
TI Factorized	Babbush et al.(2018) [1]	$\mathcal{O}(n + \log(\frac{n^2}{\epsilon}))$	$\mathcal{O}(n^2)$	$\mathcal{O}(n + \log(\frac{1}{\epsilon}))$	$\mathcal{O}(n)$
	This paper	$\mathcal{O}(n + \tilde{\lambda}_2 \log(\frac{n \eta}{\epsilon}))$	$\mathcal{O}(n \eta)$	$\mathcal{O}(n \log \eta + \frac{n}{\lambda_2} + \tilde{\lambda}_2 \log(\frac{n \eta}{\epsilon}))$	$\mathcal{O}(n \log \eta + \frac{n}{\lambda_2} + \log \tilde{\lambda}_2)$
Localized	Wan (2021) [3]	$\mathcal{O}(n)$	$\mathcal{O}(n^2)$	$\mathcal{O}(n) + \text{PREP}$	$\mathcal{O}(n) + \text{PREP}$
	This paper	$\tilde{\mathcal{O}}(n + \tilde{\lambda}_3 \log(\frac{n^2}{\epsilon}))$	$\mathcal{O}(n^2 \log^2(\frac{n^2}{\epsilon}))$	$\tilde{\mathcal{O}}(n \log \eta + \frac{n^2}{\lambda_3} \log(\frac{n^2}{\epsilon}) + \tilde{\lambda}_3 \log(\frac{n^2}{\epsilon}))$	$\mathcal{O}(n \log \eta + \frac{n^2}{\lambda_3} \log(\frac{n^2}{\epsilon}) + \log \tilde{\lambda}_3)$

(b) Fixed η -particle subspace.

TABLE II: Comparison of input-model cost for second-quantized electronic Hamiltonians with precision ϵ . Here n is the number of spin orbitals and η is the number of particles in the states considered. The parameters λ_i and $\tilde{\lambda}_i$ are free integers used in [43], with ranges $\lambda_1, \tilde{\lambda}_1 \in [1, n^4]$, $\lambda_2, \tilde{\lambda}_2 \in [1, n]$, $\lambda_3 \in [1, n^2 \log^2(\frac{n^2}{\epsilon})]$, and $\tilde{\lambda}_3 \in [1, n^2 \log^2(\frac{\eta^2}{\epsilon})]$. Each row corresponds to the input model constructed in a paper. We use N/A to indicate that the cost is not applicable for [2], as that work focuses on Trotter-based simulation without an explicit input-model construction. PREP denotes the cost of the PREPARE oracle, since [3] mainly analyzes the SELECT oracle.

controlling qubit is used to select one of the O_B oracle (O_B^1 or O_B^2) circuits. The output states of the O_B^1 or O_B^2 circuit are used as the $|b_0\rangle$ and $|b_1\rangle$ input to the direct sampling circuit discussed earlier and shown in Fig. 14. In addition to these inputs, the qubits initialized with the second $|0^{m_b-1}\rangle$ and $|0\rangle$ are also taken as the input to the direct sampling oracle.

The ancilla qubits that are used as the input to both the data lookup and direct sampling oracles are uncomputed to $|0\rangle$ and $|0^{m_b-1}\rangle$ states after they are used in the first data lookup circuit and direct sampling oracle with another data lookup oracle O_B^1 . The controlling qubit at the top of the circuit is reset to $|0\rangle$ by an additional application of the $p \neq q$ check oracle applied at the beginning of the circuit. We post-select validation qubit to be in state $|0\rangle$ in order to construct linear combination of non-vanishing one-body interactions. As usual, the qubits used to encode the indices of the interaction terms were post-selected to $|0\rangle$. To be clear, all ancilla qubits require post-selection has a measurement procedure in the end of the circuit and all other ancilla qubits are uncomputed to be in $|0\rangle$.

Using the resource estimates for the SELECT-SWAP and SWAP-UP oracles from Sec. V A, we obtain the overall complexity of the input model. The sparsity oracle O_C introduced in Sec. IV C requires at most eight SWAP-UP

operations in O_s and four SWAP-UP operations in O_ϕ , illustrated in Fig. 6a and Fig. 5. Since the ladder operation in O_ϕ does not include T gates. The block encoding requires $13n + \mathcal{O}(\log(n))$ qubits, $96n + \mathcal{O}(\log(n))$ T gates count and $12 \log(n)$ T depth.

The amplitude oracle O_A is constructed through two data lookup oracle O_B^1 and O_B^2 . The Eqs. (56) and (57) describe the complexity of the SELECT-SWAP circuit and show that, with $L = n^2$ and $m_b = \log(\frac{n^2}{\epsilon})$, the construction of amplitude oracle requires $\lambda \log(\frac{n^2}{\epsilon})$ qubits and $8 \left\lceil \frac{n^2}{\lambda} \right\rceil + 16\lambda \log(\frac{n^2}{\epsilon})$ T gates, with T depth $\frac{n^2}{\lambda} + \log(\lambda)$. The complexity of block encoding arises from the combined costs of the sparsity oracle and the amplitude oracle.

For a general electronic Hamiltonian with two-body interaction expressed as

$$\mathcal{H} = h_{pq} a_p^\dagger a_q + h_{pqrs} a_p^\dagger a_q^\dagger a_r a_s, \quad (62)$$

and labeled as General in Table IIa, we similarly require $\mathcal{O}(\lambda m_b)$ qubits and

$$\mathcal{O}\left(n + \left\lceil \frac{L}{\lambda} \right\rceil + \lambda m_b\right) \quad (63)$$

T gates with

$$\mathcal{O}\left(n + \frac{L}{\lambda} + 2\log(\lambda)\right) \quad (64)$$

T depth. By tuning λ in the range of $[1, L]$, we can obtain a block encoding with optimal T gate count in our method,

$$\mathcal{O}\left(n + \sqrt{Lm_b}\right), \quad (65)$$

and it generates a circuit of T depth

$$\mathcal{O}\left(n + \sqrt{Lm_b}\right). \quad (66)$$

The resource required for the block encoding is summarized within Table I with λ parameter and within Table II with optimal λ for reducing the total T gate count. We emphasize that no structure is assumed for the h_{pq} or h_{pqrs} , and these coefficients are of $\mathcal{O}(1)$.

Ultimately, we analyze the Clifford gate cost and circuit depth associated with block encoding. Recent advances have significantly reduced the overhead of fault-tolerant implementation of the T gate [61, 62]. Looking ahead, it is possible that the fault-tolerant costs of Clifford and T gates may become comparable. In such a regime, the Clifford gate count will also play a crucial role in evaluating the efficiency of quantum algorithms.

The Clifford gate cost of the block encoding for Hamiltonian is $Lm_b + o(L)$ based on the complexity analysis in Sec. V and [43]. The leading term Lm_b comes from the control multi-NOT gate (defined as a generalization of the CNOT gate with control on a single qubit and NOT on a few other qubits) within the SELECT-SWAP circuit. These gates could also potentially contribute to the main circuit depth. Note that within our block encoding circuit, there are two components likely to contribute to the main circuit depth. The ladder operators within O_ϕ can be implemented with circuit depth n . However, as discussed earlier in Sec. V A, these two circuits can be implemented with $\mathcal{O}(1)$ depth with the same gate cost.

Compared to the Jordan-Wigner transform based method [3], the number of SWAP-UP used in the algorithm is smaller. This phenomenon can be understood through each creation operator and annihilation operator can be decomposed into a combination of two Pauli strings. For structured Hamiltonian, where the sparsity oracle contribute to the main Clifford cost, the proposed block encoding requires less Clifford gate cost.

VII. BLOCK ENCODING FOR η -PARTICLE HAMILTONIAN

The block encoding scheme discussed above in Sec. IV and Sec. V for the Hamiltonian given by Eq. (20) introduces a subnormalization factor L that is proportional to n^4 where n is the number of orbitals required to represent

the Hamiltonian. Such a subnormalization factor results from using the diffusion operator to generate suppositions of all possible $ijkl$ combinations. Because Eq. (20) can be block diagonalized by basis states that preserve particle number, one would expect that the block encoding for a diagonal block of the Hamiltonian associated with a fixed particle number η will have a small subnormalization factor.

In this section, we show that this is indeed the case. We present an efficient quantum circuit for block encoding the η -particle block of the Eq. (20). We show that the subnormalization factor associated with this block encoding circuit is $\eta^2 n^2$, which can be much smaller than n^4 when $\eta \ll n$.

A. Indirect diffusion

The key idea we use to reduce the subnormalization factor is to use an indirect diffusion oracle to generate a subset of indices associated with an annihilation operator in Eq. (20). Note that, if $|j\rangle$ is an η -particle state, i.e., η of the n orbitals are occupied, η qubits of the n -qubit representation of $|j\rangle$ are in the $|1\rangle$ state while others are in the $|0\rangle$ state. The only relevant annihilation operators are those that annihilate the occupied orbitals. Therefore, the indirect diffusion oracle is devised to indirectly generate a superposition of the indices of the occupied orbitals associated with $|j\rangle$.

Let us use $add_i(j)$ to represent the bit index of the i th occupied qubit in $|j\rangle$. For example, if $n = 4$ and $\eta = 2$ and $|j\rangle = |0101\rangle$, then $add_0(j) = 1$ and $add_1(j) = 3$. The implementation of an indirect diffusion oracle hinges on constructing an oracle that can be used to map $|i\rangle$ and j to $add_i(j)$. We will refer to such an oracle as an *occupation detection oracle* and denote it by O_{occ} throughout the paper. The operation performed by O_{occ} can formally be expressed as

$$|i\rangle |0^{\log(n)}\rangle |j\rangle \xrightarrow{O_{occ}} |i\rangle |add_i(j)\rangle |j\rangle, \quad (67)$$

and

$$|i\rangle |add_i(j)\rangle |j\rangle \xrightarrow{O_{occ}} |i\rangle |0^{\log(n)}\rangle |j\rangle. \quad (68)$$

By composing a standard Hadamard diffusion operator that performs the following operation

$$|0^{\log(\eta)}\rangle |0^{\log(n)}\rangle |j\rangle \xrightarrow{H^{\otimes \log(\eta)}} \frac{1}{\sqrt{\eta}} \sum_{i=0}^{\eta-1} |i\rangle |0^{\log(n)}\rangle |j\rangle, \quad (69)$$

to generate a superposition of $|i\rangle$'s for $i = 0, 1, 2, \dots, \eta - 1$ with the oracle shown in Eq. (67), we obtain the indirect diffusion oracle O_{IDF} that yields the following mapping,

$$|0^{\log(\eta)}\rangle |0^{\log(n)}\rangle |j\rangle \xrightarrow{O_{IDF}} \frac{1}{\sqrt{\eta}} \sum_{i=0}^{\eta-1} |i\rangle |add_i(j)\rangle |j\rangle. \quad (70)$$

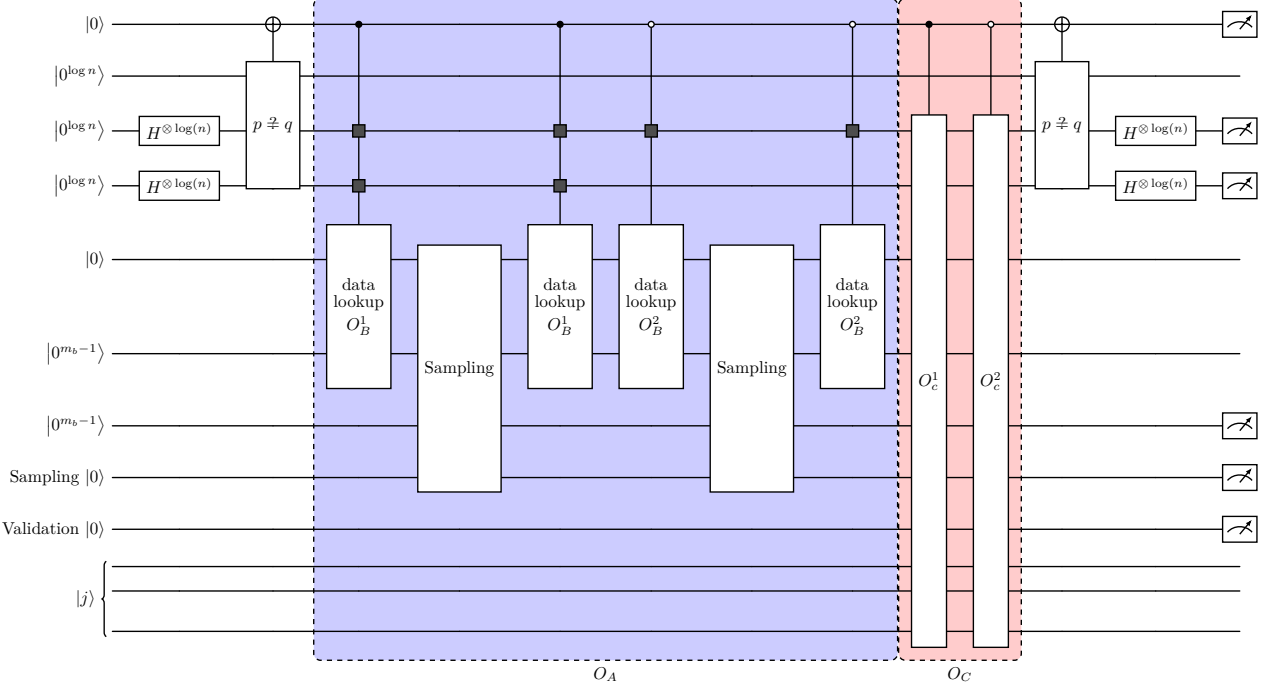


FIG. 15: Illustration of a quantum circuit for block encoding of one-body Hamiltonian.

Note that, unlike the standard diffusion operator that take $|0^{\log(\eta)}\rangle$ as the only input, the input to O_{IDF} consists of both $|0^{\log(\eta)}\rangle$ and $|j\rangle$, i.e., it depends on $|j\rangle$. The $|j\rangle$ dependency of the diffusion has a direct consequence on how the block encoding of the η -particle Hamiltonian is constructed. The indirect diffusion operator can be easily generalized to include multiple qubit registers as the input. For example,

$$|0^{\log(\eta)}\rangle |0^{\log(\eta)}\rangle |0^{\log(n)}\rangle |0^{\log(n)}\rangle |j\rangle \xrightarrow{O_{\text{IDF}}} \frac{1}{\sqrt{n\eta}} \sum_{i=0}^{\eta-1} |i_1\rangle |i_2\rangle |add_{i_1}(j)\rangle |add_{i_2}(j)\rangle |j\rangle \quad (71)$$

performs an indirect diffusion to generate a superposition of pairs of quantum states representing indices of creation and annihilation pairs that preserve the η -particle number in $|j\rangle$.

B. State-dependent O_C and O_A oracles

The superposition of states representing indices of the annihilation operators that preserve the particle number of an η -particle basis state $|j\rangle$ can be used as the input to a pair of O_A and O_C oracles to block encode an η -particle Hamiltonian.

To illustrate how these oracles are constructed, we first use the block encoding of the one-body term of the Hamiltonian Eq. (37) as an example.

To construct the AMPLITUDE oracle O_A , we follow the same technique presented in Sec. V to use a O_B oracle first to create a finite precision binary representation of each one-body matrix element $h_{i_1,add_{i_2}(j)}$. Instead of applying O_B to $|i_1\rangle |i_2\rangle$ and $|0^r\rangle$ for a general one-body term, we apply O_B to $|i_1\rangle |add_{i_2}(j)\rangle |0^r\rangle$ using the SELECT-SWAP circuit presented in Sec. V. Due to the dependency of $|add_{i_2}(j)\rangle$ on $|j\rangle$, the output of such an oracle is state $|j\rangle$ dependent. Similar to what is used in the O_A oracle for the general Hamiltonian, the binary representation of selected one-body matrix elements is then turned into amplitude factors through a direct sampling oracle O_S discussed in Sec. V B.

To start, apply O_B and O_S to the state

$$\frac{1}{\sqrt{n\eta}} \sum_{i_1=0}^{n-1} \sum_{i_2=0}^{\eta-1} |i_1\rangle |i_2\rangle |add_{i_2}(j)\rangle |0^{m_b}\rangle |0^{m_b-1}\rangle |0\rangle |j\rangle. \quad (72)$$

which is produced by the indirect diffusion operator O_{IDF} applied to the input

$$|0^{\log(n)}\rangle |0^{\log(\eta)}\rangle |0^{\log(n)}\rangle |0^{m_b}\rangle |0^{m_b-1}\rangle |0\rangle |j\rangle, \quad (73)$$

yields

$$\frac{1}{\sqrt{n\eta}} \sum_{i_1=0}^{n-1} \sum_{i_2=0}^{\eta-1} |i_1\rangle |i_2\rangle |add_{i_2}(j)\rangle |0^{m_b}\rangle |0^{m_b-1}\rangle \left(h_{i_1,add_{i_2}(j)} |0\rangle + \sqrt{1 - h_{i_1,add_{i_2}(j)}^2} |1\rangle \right) |j\rangle. \quad (74)$$

We can now apply the SPARSITY oracle O_C introduced

$$\frac{1}{\sqrt{n\eta}} \sum_{i_1, i_2} (-1)^{d_{j, i_1, add_{i_2}}} |o(j, i_1, add_{i_2})\rangle |i_1\rangle |i_2\rangle |add_{i_2}\rangle |0^{m_b}\rangle |0^{m_b-1}\rangle \left(h_{i_1, add_{i_2}} |0\rangle + \sqrt{1 - h_{i_1, add_{i_2}}^2} |1\rangle \right) |\text{FLIP}(j, i_1, add_{i_2})\rangle. \quad (75)$$

In order to ensure Eq. (13) is satisfied, we need to use a uncompute oracle to turn $|i_1\rangle$, $|i_2\rangle$, $|add_{i_2}\rangle$ to $|0^{\log(n)}\rangle$, $|0^{\log(\eta)}\rangle$ and $|0^{\log(\eta)}\rangle$ respectively. For a general one-body term, the uncompute can be accomplished by the same Hadamard diffusion operator used to generate a superposition of indices i_1 and i_2 of the creation and annihilation operators. However, because the indirect diffusion operator O_{IDF} is j dependent, we cannot use it to turn $|add_{i_2}\rangle$ back to $|0^{\log(n)}\rangle$ (uncompute) once $|j\rangle$ has been changed to $|\text{FLIP}(j, i_1, add_{i_2})\rangle$ in Eq. (75).

Therefore, additional effort is needed to construct a desired uncompute operator. One way to overcome this difficulty is to use another register to hold a copy of $|j\rangle$ that will not be altered by the O_C oracle and use this register to uncompute $|add_{i_2}\rangle$ according to Eq. (68). We should also note that making an additional copy of $|j\rangle$, which is a computational basis that can be generated by using a sequence of CNOT gates placed on matching qubits in $|j\rangle$ and $|0^{\log(n)}\rangle$ to yield

$$|j\rangle |0^{\log(n)}\rangle \rightarrow |j\rangle |j\rangle, \quad (76)$$

does not violate the well-known *no-cloning theorem*. Consider an example where $j = 01$ (a 2-bit string). Our

in Sec. IV to qubits holding $|i_1\rangle |add_{i_2}\rangle |j\rangle$ in Eq. (74) to obtain

goal is to produce:

$$|0\rangle |1\rangle |0\rangle |0\rangle \rightarrow |0\rangle |1\rangle |0\rangle |1\rangle, \quad (77)$$

where the first two qubits are initialized as $|0\rangle |1\rangle$ (representing j), and the last two start as $|0\rangle |0\rangle$. To accomplish this, we apply two CNOT gates: the first with the first qubit as control and the third as target, and the second with the second qubit as control and the fourth as target. After these operations, the third and fourth qubits will match the first and second, respectively, successfully copying the state of $|j\rangle$ onto a second register. We note that the copy operation described here is, in fact, an application of the exclusive OR (XOR) operator, as will be discussed in the next paragraph.

We could apply the O_{occ} oracle to qubits holding $|i_2\rangle$, $|add_{i_2}(j)\rangle$ and the first $|j\rangle$ according to Eq. (68) to turn $|add_{i_2}(j)\rangle$ to $|0^{\log(n)}\rangle$. The qubits holding $|i_1\rangle$ and $|i_2\rangle$ can be restored to $|0^{\log(n)}\rangle$ and $|0^{\log(\eta)}\rangle$ respectively by applying the standard Hadamard diffusion operator.

However, we still need to turn the qubits holding the copied $|j\rangle$ back to $|0^{\log(n)}\rangle$. This is not easy to do without additional resources. To overcome this difficulty, we use CNOTs applied to matching qubits in $|\text{Flip}(j, i_1, add_{i_2})\rangle$ and $|j\rangle$ to set all qubits holding $|j\rangle$ to $|0\rangle$ except the i_1 th and the add_{i_2} th qubits, which are in the $|1\rangle$ state because $|\text{Flip}(j, i_1, add_{i_2})\rangle$ and $|j\rangle$ differ only in these qubits, i.e., a circuit is constructed to perform

$$|\text{Flip}(j, i_1, add_{i_2})\rangle |j\rangle \rightarrow |\text{Flip}(j, i_1, add_{i_2})\rangle |\text{Flip}(j, i_1, add_{i_2}) \oplus j\rangle, \quad (78)$$

where \oplus is the exclusive OR operator (denoted as XOR in our quantum circuits).

We can now focus on turning the i_1 th and the $add_{i_2}(j)$ th qubits in the register holding $|\text{Flip}(j, i_1, add_{i_2}) \oplus j\rangle$ to $|0\rangle$. To turn the i_1 th qubit of this register to $|0\rangle$, we can use the SWAP-UP circuit (SW) defined by Eq. (43) and shown in Fig. 5 to move the $|1\rangle$ state in the i_1 th qubit to the leading qubit of the register. Applying an X gate on this qubit followed by using SW^\dagger to move the resulting $|0\rangle$ back to the i_1 th qubit of the register achieves our goal.

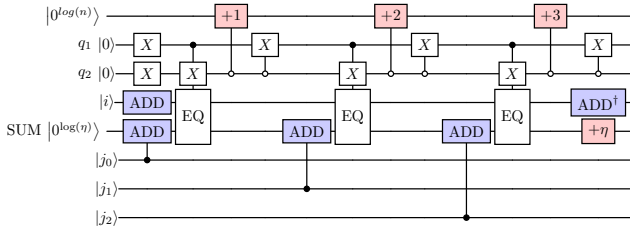
With only the $add_{i_2}(j)$ qubit of this register in $|1\rangle$, we can turn this register as well as the one holding $|add_{i_2}(j)\rangle$ to $|0^n\rangle$ and $|0^{\log(n)}\rangle$ respectively by using a slight modifi-

cation of the O_{occ} circuit that we will describe in the next section. We will refer to this special uncompute oracle circuit as O_{uc} .

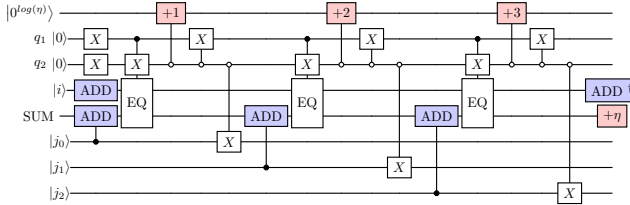
C. The implementation of O_{occ}

In this section, we describe how to construct quantum circuits to implement the O_{occ} oracle defined in Eq. (67). We also show how such an oracle can be easily modified to uncompute the qubits holding $|add_{i_2}(j)\rangle$ and the $add_{i_2}(j)$ -th qubit in the register holding $|\text{Flip}(j, i_1, add_{i_2}) \oplus j\rangle$ as we discussed in the previous section.

The basic idea is to construct a circuit to scan each qubit in the register holding $|j\rangle$ in order by using a sequence of controlled adder gates to increment a separate register (labeled as SUM in Fig. 16a) holding $\log(\eta)$ ancilla qubits that serve to record the number of qubits that have been identified to hold a $|1\rangle$ state in $|j\rangle$. When the integer value represented by the SUM register matches the integer value represented by $|i+1\rangle$, which indicates that the i th qubit in $|j\rangle$ is in the $|1\rangle$ state, we can then return the position of this $|1\rangle$ state in $|j\rangle$ (from the register at the top of the circuit in Fig. 16a), which is equivalent to the number of qubits in $|j\rangle$ that have been scanned. To keep track of the number of qubits that have been scanned, we use a separate controlled adder to change the register initialized to $|0^{\log(n)}\rangle$ to $|add_i(j)\rangle$. Two additional ancilla qubits (labeled by q_1 and q_2 in Fig. 16a) are used to set proper controls so that only one of the adders is applied for each i when the value represented by the SUM register equals $i+1$. The latter condition is checked by a comparison circuit labeled by EQ in Fig. 16a. Both the q_1 and q_2 qubits are initially set to $|1\rangle$. The q_2 qubit is flipped to $|0\rangle$ when EQ returns $|1\rangle$ and q_2 is in $|1\rangle$. It is then used to activate the adder on the leading qubits and resetting of the q_1 qubit back to $|0\rangle$.



(a) Occupation detection oracle O_{occ} .



(b) Uncompute of the occupation detection oracle O_{uocc} .

FIG. 16: Occupation detection oracle and its uncompute for the computational basis $|j\rangle$ as a η -particle state.

The O_{occ} circuit can be modified slightly to restore the $|add_i(j)\rangle$ state produced from the O_{occ} oracle as well as the $|j\rangle$ input to O_{occ} to $|0^{\log(n)}\rangle$ for a general one-body interaction. The modified circuit for such an oracle, which we denote by O_{uocc} , is shown in Fig. 16b. As we discussed in Sec. VII B, the O_{uocc} oracle is designed for a specific case when $|j\rangle$ only a few bits of a binary string are nonzero. For one-body interactions, j has one only one digit 1 in its binary representation and it is on the add_0 -th bit, then the action of the uncompute oracle O_{uocc} on

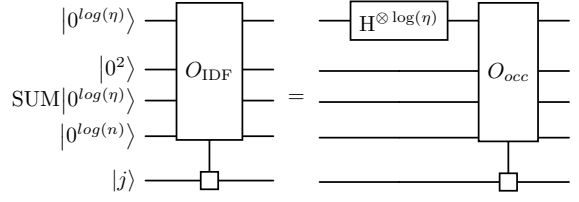


FIG. 17: Quantum circuit of indirect diffusion oracle.

the state is

$$O_{uocc} |add_0(j)\rangle |j\rangle = |0^{\log(n)}\rangle |0^n\rangle, \quad (79)$$

where $|j\rangle = |0 \dots 01 \dots 0\rangle$. Similar to the O_{occ} oracle where the oracle computes the index for the first occupied qubit within $|j\rangle$ and adds $add_0(j)$ to $add_0(j)$. This process uncomputes $add_0(j)$. Within the construction of O_{uocc} , we use a Pauli X gate to uncompute $|j\rangle$ whenever $add_0(j)$ -th qubit is found.

We now estimate the number of T gates required in the circuit implementation of O_{occ} and O_{uocc} and their T depth. Each ADD subcircuit requires $\mathcal{O}(\log(\eta))$ T gates and has a T depth of $\mathcal{O}(\log(\eta))$ [63]. The EQ operation can be implemented by using a sequence of CNOT gates to check whether each qubit in the register holding $|i\rangle$ and the register labeled by SUM is in the same state. When that is the case and the state on q_1 qubit equals to $|0\rangle$, a NOT is applied to qubit q_2 . This operation can be implemented with $\mathcal{O}(\log(\eta))$ T gates in a circuit that has a T depth of $\mathcal{O}(\log \log(\eta))$. One clean ancilla is used in such a circuit. In total, these two oracles require $\mathcal{O}(n \log(\eta))$ T gates and have a T depth of $\mathcal{O}(n \log(\eta))$.

D. The complete circuit for η -particle Hamiltonian

We now show how the indirect diffusion and state-dependent O_A and O_C oracles fit together in a complete quantum circuit implementation of the block encoding of an η -particle Hamiltonian.

Again, we use the Hamiltonian Eq. (37) that contains only one-body interactions as an example to illustrate how the entire circuit is constructed. Extension to an η -particle Hamiltonian that contains both one-body and two-body interactions is relatively straightforward.

In the circuit shown in Fig. 18, Hadamard gates are used to generate a superposition of the indices (p) for the creation operator a_p^\dagger . The indirect diffusion oracle O_{IDF} , which takes $|0^{\log(n)}\rangle$ and $|0^{\log(n)}\rangle$ as the input in addition to $|j\rangle$, is used to generate the superposition of selected q indices associated with valid annihilation operators for the state $|j\rangle$, i.e., the q 's that satisfy $a_q |j\rangle \neq 0$. The O_A circuit block contains both the SELECT-SWAP based data lookup circuit gadgets and direct sampling based circuit gadgets to encode the numerical value of h_{pq} for selected q 's. (We note that the data lookup circuit itself still stores all the classical data encoding the

coefficients for all p, q pairs.) Note that the inputs to O_A include the superposition of p 's at the top circuit and selected q 's returned from O_{IDF} as well as the qubits initialized with $|0^{m_b}\rangle$ and $|0^{m_b-1}\rangle$, the ancilla qubit labeled by ‘Sampling’. To the right of the O_A circuit block is an O_{occ} circuit used to restore the qubits holding the superposition of a subset of indices (q) of valid annihilation operators for the state $|j\rangle$ to $|0^{\log(n)}\rangle$. However, such an uncomputing operation is not necessary in the overall circuit because the superposition of selected q 's is needed again in the O_C oracle circuit. Instead of using another O_{occ} to regenerate such a superposition from the uncomputed qubits, we can simply remove the two O_{occ} circuit blocks together between the O_A and O_C in Fig. 18 cancel with each other. We display them Fig. 18 merely to show how the O_A and O_C circuit blocks can be assembled in the overall circuit.

The XOR circuit block to the left of the O_C circuit block is used to implement Eq. (76). The O_C takes the valid indice (p, q) -pair, denoted as $\{(i_1, \text{add}_{i_2}(j)) \mid 0 \leq i_1 \leq n-1, 0 \leq i_2 \leq \eta-1\}$ on qubits labeled with p, q as input and turn the state $|j\rangle$ into $|\text{Flip}(j, i_1, \text{add}_{i_2})\rangle$. In addition, it keeps the validation qubit in state $|0\rangle$ if $a_{i_1}^\dagger a_{\text{add}_{i_2}(j)} |j\rangle \neq 0$ and otherwise turn the state from $|0\rangle$ to $|1\rangle$. By another XOR operation, we duplicate the state $|\text{Flip}(j, i_1, \text{add}_{i_2})\rangle$ to the n qubits at the bottom of the circuit. For l -th qubit within these two quantum register, the if $|\text{Flip}(j, i_1, \text{add}_{i_2})\rangle_l = |j\rangle_l$, then after the XOR operation, the state equals $|0\rangle$ on l -th qubit within the last n qubits at the bottom of the circuit. For this quantum register, only the i_1 and $\text{add}_{i_2}(j)$ qubit in state $|1\rangle$.

The SW-X circuit block (a SWAP-UP and its inverse with an X gate in between) follows the second XOR circuit block is used to turn the i_1 th qubit in the register holding $|\text{Flip}(j, i_1, \text{add}_{i_2}) \oplus j\rangle$ to $|0\rangle$ as we discussed in Sec. VII B

The O_{uocc} circuit block that follows turns the $\text{add}_{i_2}(j)$ th qubit in the same register to $|0\rangle$ and effectively turning entire register previously holding $|\text{Flip}(j, i_1, \text{add}_{i_2}) \oplus j\rangle$ is set to $|0^{\log(n)}\rangle$.

At the end of the circuit, Hadamard gates are used to reset the two registers at the top of the circuit to $|0^{\log(n)}\rangle$ and $|0^{\log(\eta)}\rangle$ respectively.

We now analyze the gate complexity of the block encoding circuit for an η -particle Hamiltonian. We use $2\log(n) + 2\log(\eta)$ Hadamard gates to create superposition of indices. The gate count for O_{uocc} and O_{occ} differs merely by a small constant factor η for Clifford gate. If we simplify the circuit by dropping two O_{occ} with in the circuit, we use the oracle twice. Based on the discussion Sec. VII C, the O_{occ} circuit uses $\mathcal{O}(n\log(\eta))$ T gates and has a T depth of $\mathcal{O}(n\log(\eta))$. The direct sampling oracle contains $\mathcal{O}(m_b)$ T gates, as we discussed in Sec. V B. This subcircuit block contributes a minor addition to the total T count in the entire circuits.

The major contributing factor to the gate complexity comes from the sparsity oracle O_C and amplitude oracle

O_A . The O_C circuit uses $\mathcal{O}(n)$ T gates and has a T-depth of $\mathcal{O}(\log(n))$ as discussed in Sec. IV C. The O_A oracle requires $\mathcal{O}(\frac{L}{\lambda} + \lambda m_b)$ T gates and has a T-depth of $\mathcal{O}(\frac{L}{\lambda} + \log(\lambda))$. Therefore, the total T gate count is

$$\mathcal{O}\left(n\log(\eta) + \frac{L}{\lambda} + \lambda m_b\right). \quad (80)$$

The T-depth is

$$\mathcal{O}\left(n\log(\eta) + \frac{L}{\lambda} + \log(\lambda)\right). \quad (81)$$

By tuning λ in the range of $[1, L]$, we can obtain a block encoding with optimal T gate count

$$\mathcal{O}\left(n\log(\eta) + \sqrt{Lm_b}\right), \quad (82)$$

which generates a circuit with T depth

$$\mathcal{O}\left(n\log(\eta) + \sqrt{Lm_b}\right). \quad (83)$$

We next clarify the meaning of L in the context of the O_A oracle, as well as the subnormalization factor and the requirement on m_b for the block encoding of an η -particle sector of the Hamiltonian. For a general one-body Hamiltonian, there are in total n^2 terms. However, for each η -particle state $|j\rangle$, only a subset of all one-body interactions $a_p^\dagger a_q^\dagger$ contribute non-vanishing matrix elements. The number of coefficients associated with these non-vanishing terms for a given state $|j\rangle$ scales as $\mathcal{O}(n\eta)$. These coefficients must be loaded by the O_A oracle. Nevertheless, to ensure that the coefficients for all η -particle states can be accessed, the total number of data entries stored in the data-lookup table must still be $L = n^2$.

The subnormalization factor and the requirement on m_b depend on the number of valid terms associated with the η -particle states. This number equals the total number of terms in the block encoding of the full Hamiltonian, but differs when restricted to a specific η -particle sector. For each η -particle number state $|j\rangle$, the number of valid Hamiltonian terms scales as $\mathcal{O}(n\eta)$. Recall that the subnormalization factor originates from the LCU construction and scales proportionally to the number of valid terms for the state $|j\rangle$. In our case, the subnormalization factor equals $\mathcal{O}(n\eta)$. Furthermore, to achieve an ϵ -accurate block encoding, each valid term must be specified with precision ϵ/η , which leads to the requirement

$$m_b = \mathcal{O}\left(\log\left(\frac{\eta}{\epsilon}\right)\right) \neq \mathcal{O}\left(\log\left(\frac{L}{\epsilon}\right)\right). \quad (84)$$

In addition to the qubits shown in Fig. 18, λm_b qubits are used for data lookup. Therefore, the total number of qubits required in the block encoding circuit for the one-body component of the Hamiltonian is $2n + 2\log(n) + \log(\eta) + 2m_b + 2 + m_b + \lambda m_b$.

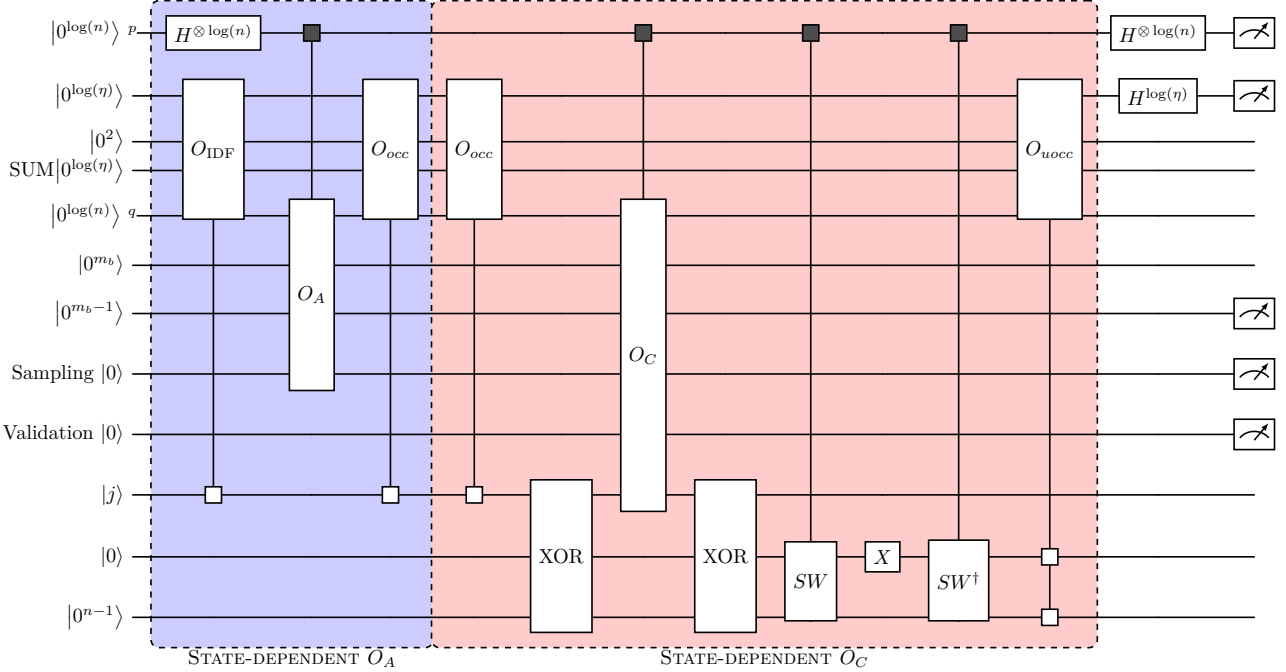


FIG. 18: The block encoding quantum circuit of an η -particle one-body operator.

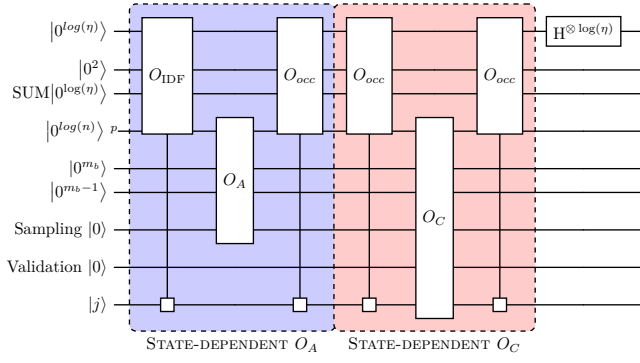


FIG. 19: The quantum circuit of the block encoding of an η -particle number operator.

When $p = q$, the one-body term is a number operator. The block encoding circuit for this term can be simplified considerably, as illustrated in Fig. 19. We are only concerned with p 's that are generated from the indirect diffusion oracle. We note that in Fig. 19 the circuit convention is modified a bit. The input or control on the qubit label by p for amplitude oracle or sparsity oracle is included in O_A and O_C .

Because the number operator does not alter the state $|j\rangle$ and there is no phase factor to be considered, there is no need to replicate $|j\rangle$ as in the case when $p \neq q$. Furthermore, there is no need to construct additional circuit blocks to uncompute ancilla qubits.

Similar to the discussion for the block encoding for general one-body interaction, the T gate count and T depth follow same estimate shown in Eq. (81) and Eq. (80) but

with $L = n$ and $m_b = \log(\frac{\eta}{\epsilon})$.

For the general η -particle electronic Hamiltonian Eq. (62) where $L = n^4$ and $m_b = \log(\frac{n^2\eta^2}{\epsilon})$, the construction of block encoding circuit requires a data lookup oracle that is much in circuit size to store the quantum data and with same formulas shown in Eq. (81) and Eq. (80). The overall complexity is summarized in the row labeled *general* in Table IIa. In total, the block encoding requires

$$\mathcal{O}\left(n \log(\eta) + \frac{n^4}{\lambda} + \lambda \log\left(\frac{1}{\epsilon}\right)\right) \quad (85)$$

T gates and

$$\mathcal{O}\left(n \log(\eta) + \frac{n^4}{\lambda} + \log(\lambda)\right) \quad (86)$$

T depth, where λ ranges from 1 to n^4 . Including the dominant Clifford cost for loading classical data, $Lm_b = n^4 \log\left(\frac{n^2\eta^2}{\epsilon}\right)$, the total Clifford gate count becomes

$$\mathcal{O}\left(n \log(\eta) + \frac{n^4}{\lambda} + m_b \lambda + n^4 m_b\right). \quad (87)$$

VIII. BLOCK ENCODING FOR STRUCTURED HAMILTONIAN

It follows from the discussions in Sec. VI that, for a general second-quantized Hamiltonian, the number of Clifford and T-gates required to construct the O_A oracle

circuit typically exceeds that required for the O_C oracle. Without additional assumptions on the second quantized Hamiltonian, the O_A oracle circuit shown previously is nearly optimal with respect to the Clifford+T gates usage [64]. The majority of Clifford gates are used in the decomposition of the controlled multi-qubit Pauli X gate in the data-lookup oracle. The total number of CNOT gates required is $n^4 m_b + o(n^4 m_b)$. By tuning the parameter λ in the SELECT-SWAP structure, the total number of T gates required is reduced to $\mathcal{O}(\sqrt{n^2 m_b})$. This optimization minimizes the fault-tolerant resource cost for the data-lookup oracle, making the gate complexity approach the theoretical lower bound for T gate usage for general state preparation tasks [64].

However, the coefficients of the creation and annihilation operators in some Hamiltonians have additional structures that can be leveraged to reduce the circuit complexity. In particular, if some of these coefficients are small, which leads to a reduced number of, for example, two-body interaction terms, a simpler data-lookup oracle circuit can be constructed to reduce the gate complexity of the overall circuit.

In this section, we focus on the construction of block encoding for Hamiltonians with translation invariance or small coefficients. We consider Hamiltonians both with a fixed particle number η and without such a constraint.

A. Hamiltonians with nearest-neighbor interactions

If the coefficients of the one or two-body terms are negligibly small, it is not necessary to encode these near-zero coefficients in the block encoding circuit of the Hamiltonian. By neglecting these terms, we can further reduce the subnormalization factor of the block encoding scheme and use fewer resources in the data lookup circuit.

Here we discuss how to reduce the gate complexity of block encoding for $\mathcal{H} = \sum_{p,q} h_{pq} a_p^\dagger a_q$ in which the coefficients h_{pq} decay exponentially with respect to $|p - q|$. To be specific, we assume

$$|h_{pq}| \leq C e^{-\alpha|p-q|} \quad (88)$$

for some $\alpha > 0, C > 0$. If the underlying lattice associated with the Hamiltonian is defined on a torus \mathbb{T} , the decay assumption is modified to take the form

$$|h_{pq}| \leq C e^{-\alpha \max(|p-q|, n-|p-q|)}, \quad (89)$$

where the distance accounts for the periodic boundary conditions.

The rapid magnitude decay of the coefficients h_{pq} with respect to $|p - q|$ allows us to ignore (p, q) pairs that correspond to small $|h_{pq}|$ without sacrificing the accuracy of the block encoding. To construct a block encoding with precision ϵ , it suffices to retain only the one-body interaction terms, whose indices satisfy

$$|p - q| \leq C' \log\left(\frac{n}{\epsilon}\right), \quad (90)$$

where C' is a constant independent of n and ϵ . The number of (p, q) pairs satisfying Eq. (90) scales as $\mathcal{O}(n \log(\frac{n}{\epsilon}))$. Considerably fewer one-body terms need be considered also if $|h_{pq}| \leq \frac{C}{|p-q|^\gamma}$, i.e. $|h_{pq}|$ decays algebraically with respect to $|p - q|$, or h_{pq} is nonzero only for $|p - q| = 1$. In these two scenarios, the number of coefficients to be considered is reduced to $\mathcal{O}(n(\frac{1}{\epsilon})^\gamma)$ and $\mathcal{O}(n)$ respectively.

Suppose for each index p , only $2M + 1$ terms in the Hamiltonian satisfying $|p - q| \leq M$ are retained. By retaining only these terms, we can reduce the subnormalization factor of the block encoding of such a Hamiltonian to $\mathcal{O}(nM)$ from $\mathcal{O}(n^2)$ by using an indirect diffusion operator that requires fewer Hadamard gates.

To illustrate how such an indirect diffusion circuit may be constructed, we examine a simplified case where h_{pq} is nonzero only when $|p - q| = 1$. A partial construction of block encoding for this Hamiltonian is described below, and the construction of the quantum circuit is illustrated in Fig. 20.

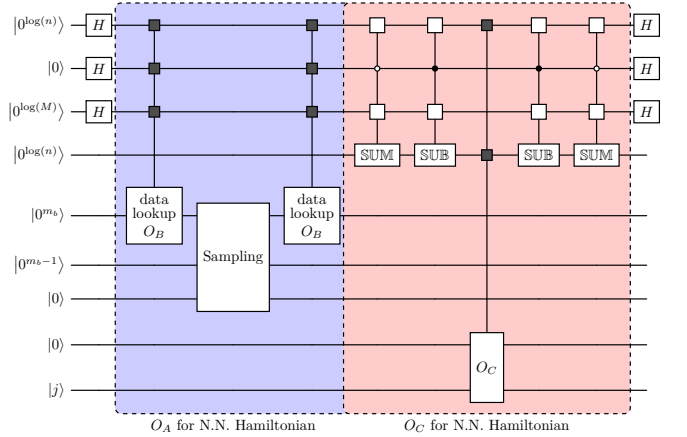


FIG. 20: Quantum circuit of block encoding for one-body Hamiltonian with Nearest-Neighbor interactions.

Intuitively, generating a superposition of $|p\rangle|p-1\rangle$ and $|p\rangle|p+1\rangle$, which represents all index pairs of $h_{p,p-1}$ and $h_{p,p+1}$ requires one qubit to represent a superposition of $|0\rangle$ and $|1\rangle$ in addition to the $\log(n)$ qubits required to represent a superposition of $|p\rangle$ for $p = 0, 1, \dots, n-1$ and another $\log(n)$ qubits used to hold superpositions of $|p-1\rangle$ or $|p+1\rangle$.

To generate a superposition of $|p\rangle|p+1\rangle$ and $|p\rangle|p-1\rangle$, we can first duplicate the first $\log(n)$ qubits used to hold the superposition of $|p\rangle$ in the second set of $\log(n)$ qubits using CNOT gates. We can then use the superposition of $|0\rangle$ and $|1\rangle$ generated in the third single qubit register to conditionally add or subtract 1 from the second set of $\log(n)$ qubits to yield

$$\frac{1}{\sqrt{2n}} \sum_{p=0}^{n-1} |p\rangle|p-1\rangle|0\rangle + \frac{1}{\sqrt{2n}} \sum_{p=0}^{n-1} |p\rangle|p+1\rangle|1\rangle. \quad (91)$$

The superposition of $|p\rangle|p+1\rangle$ and $|p\rangle|p-1\rangle$ can be easily uncomputed using the identical circuit block employed to generate such a superposition.

When $M > 1$, the superposition states,

$$\begin{aligned} & \frac{1}{\sqrt{nM}} \sum_{p=0}^{n-1} \sum_{m=1}^M |p\rangle|p-m\rangle|m\rangle|0\rangle \\ & + \frac{1}{\sqrt{nM}} \sum_{p=0}^{n-1} \sum_{m=1}^M |p\rangle|p+m\rangle|m\rangle|1\rangle. \end{aligned} \quad (92)$$

can be prepared in a similar way. To generate the state, we first generate a superposition of state

$$\frac{1}{\sqrt{nM}} \sum_{p=0}^{n-1} \sum_{m=1}^M |p\rangle|m\rangle \quad (93)$$

by applying Hadamard gates to $\log(n) + \log(M)$ qubits. We then use another qubit to prepare a superposition of $|0\rangle$ and $|1\rangle$ states which allows us to generate the superposition of both $|p-m\rangle$ and $|p+m\rangle$ on another quantum register of $\log(n)$ qubits for each fixed p and m .

The subnormalization factor resulting from Eq. (92) is nM , which is the number of terms in the M nearest neighbor one-body Hamiltonian. It is significantly less than the corresponding n^2 subnormalization factor for block encoding a general one-body Hamiltonian when $M \ll n$. The reduction in the number of terms also translates into a reduction in the number of qubits used to construct the O_B oracle with ϵ precision in Eq. (53), which is $m_b = \log\left(\frac{nM}{\epsilon}\right)$ instead of $m_b = \log\left(\frac{n^2}{\epsilon}\right)$. The number of additional T gates and Clifford gates used to perform conditional summations and subtractions for generating the superposition of $|p\rangle|p-m\rangle$ and $|p\rangle|p+m\rangle$ in Eq. (92) is

$$\mathcal{O}\left(\log\left(\frac{nM}{\epsilon}\right) + \log(n)\right) = \mathcal{O}\left(\log(n) + \log\left(\frac{1}{\epsilon}\right)\right) \quad (94)$$

as discussed in [63]. This additional cost does not contribute to the main complexity of block encoding asymptotically with respect to n , given the sparsity oracle requires $\mathcal{O}(n)$ gate complexity and ϵ required in scientific problems would typically add a small constant $\log(\frac{1}{\epsilon})$. Moreover, the number of additional gates is relatively small compared to the savings in the optimal gate complexity for implementing the structured O_C and O_A oracles, $\mathcal{O}\left(\sqrt{n^2 \log(n/\epsilon)} - \sqrt{nM \log\left(\frac{nM}{\epsilon}\right)}\right)$, which can be deduced by substituting $L = nM$ and $L = n^2$ into Eq. (65) and taking the difference. The reduction in the T depth is of the same scaling, which can also be deduced by substituting $L = n^2$ and $L = nM$ into Eq. (66).

More gains in gate complexity can be achieved for Hamiltonians that contain two-body interactions. If the number of two-body interaction terms can be reduced

from $L = n^4$ in the general case to $L = n^2M^2$ for the M nearest neighbor case, the subnormalization factors is reduced from $\mathcal{O}(n^4)$ to $\mathcal{O}(n^2M^2)$ and the reduction in T gate complexity can be calculated directly from Eq. (63). For the two-body interaction, we need to generate a superposition of states of the form $|p\rangle|p \pm m\rangle|q\rangle|q \pm m\rangle$. This process begins by preparing a superposition over all $|p\rangle|q\rangle$ states, using $2\log(n)$ Hadamard gates, followed by arithmetic circuits to perform the necessary additions and subtractions between p and m , or q and m . Compared to the one-body interaction case, the number of arithmetic operations is doubled; therefore, the overall additional cost remains $\mathcal{O}\left(\log\left(\frac{nM}{\epsilon}\right) + \log(n)\right)$. Its asymptotic complexity with respect to n is still negligible in the construction of block encoding. The number of additional gates is also smaller than the savings in the implementation of structured O_C and O_A oracles, $\mathcal{O}\left(\sqrt{n^4 \log(n/\epsilon)} - \sqrt{n^2M^2 \log\left(\frac{n^2M^2}{\epsilon}\right)}\right)$, which can be deduced by substituting $L = n^2M^2$ and $L = n^4$ into Eq. (65) and taking the difference. The reduction in the T depth is of the same scaling, which can also be deduced by substituting $L = n^4$ and $L = n^2M^2$ into Eq. (66).

If one is interested in block encoding the η -particle sector of the Hamiltonian with nearest-neighbor interactions, the indirect diffusion scheme introduced in section Sec. VII can be combined with the method discussed above to prepare the superposition of a subset of $|p\rangle|p-m\rangle$ and $|p\rangle|p+m\rangle$ states for, e.g., the one-body term that does not vanish when $a_p^\dagger a_q$ is applied to $|j\rangle$'s in which η qubits are occupied. The superposition of these states become the input to the O_A and O_C oracles.

The desired superposition is prepared by first using Hadamard gates and the O_{IDF} oracle discussed in section Sec. VII D to obtain

$$\begin{aligned} & \frac{1}{\sqrt{2M\eta}} \sum_{m=0}^{M-1} \sum_{i=0}^{\eta-1} |m\rangle|0^{\log(n)}\rangle|i\rangle|q_i(j)\rangle|0\rangle|j\rangle \\ & + \frac{1}{\sqrt{2M\eta}} \sum_{m=0}^{M-1} \sum_{i=0}^{\eta-1} |m\rangle|0^{\log(n)}\rangle|i\rangle|q_i(j)\rangle|1\rangle|j\rangle, \end{aligned} \quad (95)$$

where we use the j -dependent state $|q_i(j)\rangle$ to represent $|add_i(j)\rangle$ defined in Eq. (67) for emphasizing that this is corresponding to valid q indices in the superposition of valid (p, q) pair. Recall that in the block encoding of an η -particle Hamiltonian with one-body interaction introduced in Sec. VII, the standard procedure begins by generating a superposition over all p indices and all valid q indices. Rather than constructing a full superposition over all possible p indices, we here instead produce a superposition over states $|m\rangle = |p-q\rangle$ that specify the separation between p and q that guarantees h_{pq} is sufficiently large with respect to a truncation parameter that depends on the overall precision ϵ of the block encoding circuit. This refinement leverages the locality or decay properties of h_{pq} to reduce circuit complexity, encoding

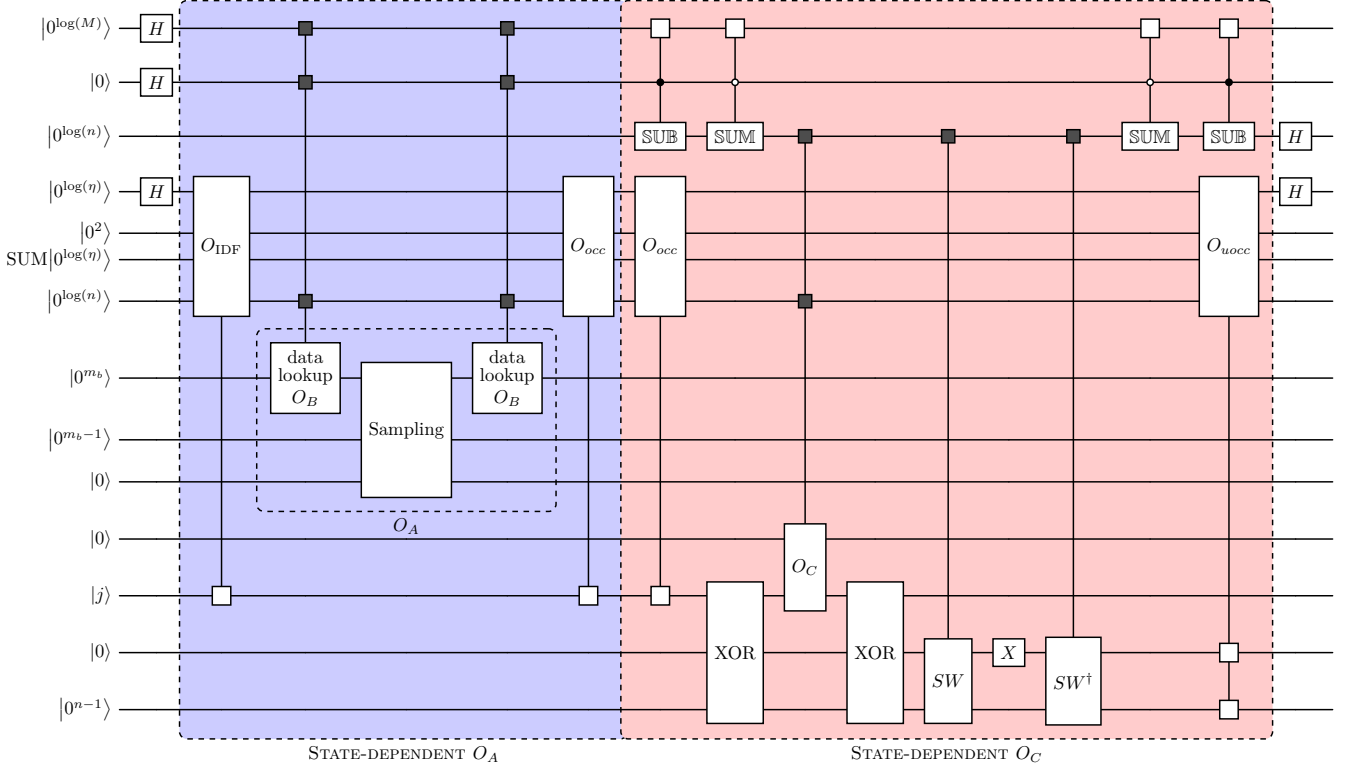


FIG. 21: Quantum circuit of block encoding for one-body η -particle Hamiltonian with nearest-neighbor interactions.

only the necessary (p, q) pairs. The superposition of the $|0\rangle$ and $|1\rangle$ states in Eq. (95) are generated to perform conditional additions and subtractions to yield a superposition of $|q_i(j) - m\rangle$ and $|q_i(j) + m\rangle$.

The O_C and O_A oracles takes

$$\begin{aligned} & \frac{1}{\sqrt{2M\eta}} \sum_{m=0}^{M-1} \sum_{i=1}^{\eta} |m\rangle |q_i - m\rangle |i\rangle |q_i(j)\rangle |0\rangle |j\rangle \\ & + \frac{1}{\sqrt{2M\eta}} \sum_{m=0}^{M-1} \sum_{i=1}^{\eta} |m\rangle |q_i + m\rangle |i\rangle |q_i(j)\rangle |1\rangle |j\rangle \end{aligned} \quad (96)$$

as well as other ancilla qubits as shown in Fig. 18 as the input to map $|j\rangle$ to $(-1)^{d_{j; q_i \pm m, q_i}} |\text{FLIP}(j; q_i \pm m, q_i)\rangle$ (the image of one-body interaction $h_{q_i \pm m, q_i} a_{q_i \pm m}^\dagger a_{q_i}$) and to encode the selected coefficients via the data lookup and direct sampling scheme discussed in Sec. V B.

In order to properly uncompute and restore ancilla qubits to $|0\rangle$ states, we need to replicate $|j\rangle$ using the same technique discussed in Sec. VII B. In addition, conditional addition and subtraction are used to restore $|q_i - m\rangle$ and $|q_i + m\rangle$ to $|0^{\log(n)}\rangle$.

For a one-body Hamiltonian, the nearest neighbor indirect diffusion produced by Eq. (96) reduces the subnormalization factor from $\mathcal{O}(n^2)$ to $\mathcal{O}(M\eta)$. Because the number of coefficients to be encoded remains to be $L = nM$, the number of qubits required to encode these coefficient to ϵ precision in data lookup is $m_b = \log\left(\frac{\eta M}{\epsilon}\right)$. It follows from Eq. (80) and Eq. (81) that the number of

T gates required in the block encoding circuit is

$$\mathcal{O}\left(n \log(\eta) + \left\lceil \frac{nM}{\lambda} \right\rceil + \lambda \log\left(\frac{\eta M}{\epsilon}\right)\right), \quad (97)$$

and the T-depth is

$$\mathcal{O}\left(n \log(\eta) + \frac{nM}{\lambda} + 2 \log(\lambda)\right) \quad (98)$$

with $1 \leq \lambda \leq nM$.

The circuit that implements the block encoding of this structured Hamiltonian is illustrated in Fig. 21.

B. Hamiltonian with translation invariance

Translation invariance is a key property in many physical systems, which may greatly simplify block encoding constructions. For Hamiltonians with translation invariance, fewer coefficients are to be encoded because they are related by spatial symmetry. This special structure results in both a smaller subnormalization factor and a cheaper data lookup oracle for encoding unique nonzero coefficients. This feature makes translation-invariant Hamiltonians particularly amenable to resource-saving quantum simulation techniques, similar to the advantages seen in nearest-neighbor interaction models.

To demonstrate how block encoding can be constructed for translation-invariant Hamiltonians, we con-

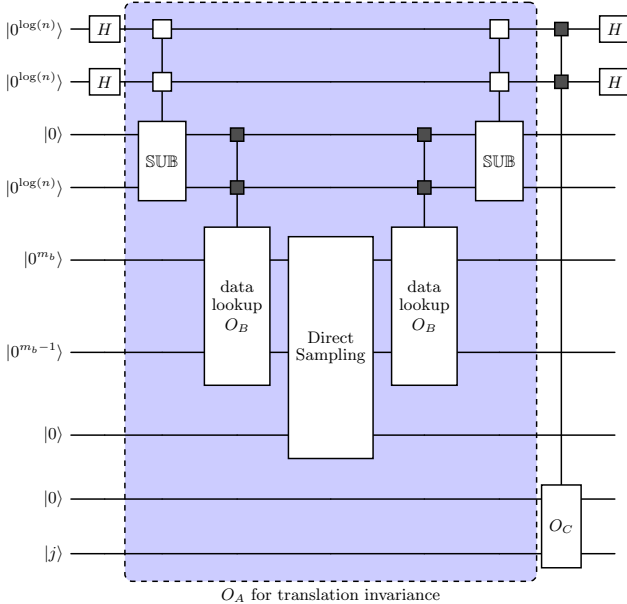


FIG. 22: Quantum circuit of block encoding for one-body Hamiltonian with translation invariance.

consider Hamiltonians that contain only one-body interactions, i.e.,

$$\mathcal{H} = \sum_{p,q=0}^{n-1} T(p-q) a_p^\dagger a_q. \quad (99)$$

Because there are at most $\mathcal{O}(n)$ nonzero coefficients $T(p-q)$ in Eq. (99), the O_A oracle can use a data lookup oracle that requires fewer resources. The key to achieve a reduction in complexity is to generate the superposition of $|p-q\rangle$ first by using arithmetic subtraction [63] and compare oracles [1] to yield

$$\frac{1}{n} \sum_{p,q=0}^{n-1} |p\rangle |q\rangle |p-q\rangle |\text{sgn}(p-q)\rangle. \quad (100)$$

The O_A oracle takes $|p-q\rangle |\text{sgn}(p-q)\rangle$ as the input to retrieve the corresponding $T(p-q)$ value encoded by a direct sampling oracle.

Because the number of coefficients is reduced to $2n-1$, the number of qubits required to implement the data lookup oracle becomes $m_b = \log(\frac{2n-1}{\epsilon})$. Substituting this m_b value and $L = 2n-1$ into Eq. (63) yields the following T gate count

$$\mathcal{O}\left(n + \left\lceil \frac{n}{\lambda} \right\rceil + \lambda \log\left(\frac{n}{\epsilon}\right)\right). \quad (101)$$

It follows from Eq. (64) that the T-depth of the block encoding circuit is

$$\mathcal{O}\left(n + \frac{n}{\lambda} + 2 \log(\lambda)\right). \quad (102)$$

By reducing L from n^2 to $2n-1$, we can achieve $\mathcal{O}\left(\sqrt{n^2 \log\left(\frac{n}{\epsilon}\right)} - \sqrt{n \log\left(\frac{n}{\epsilon}\right)}\right)$ reduction in gate complexity, which can be deduced by substituting $L = 2n-1, m_b = \log\left(\frac{2n-1}{\epsilon}\right)$ and $L = n^2, m_b = \log\left(\frac{n^2}{\epsilon}\right)$ into Eq. (65) and taking the difference. Such a reduction is significantly larger than the additional cost $\mathcal{O}(\log(n) + \log(\frac{1}{\epsilon}))$ shown in Eq. (94), required to implement the diffusion oracle used to generate the superposition of states in Eq. (100) using arithmetic subtraction and comparison oracles.

To restrict the block encoding to the η -particle sector of the Hamiltonian, we need to combine the techniques discussed above with the indirect diffusion scheme presented in Sec. V B to generate

$$\frac{1}{\sqrt{n\eta}} \sum_{p=0}^{n-1} \sum_{i=0}^{\eta-1} |p\rangle |i\rangle |q_i\rangle |p-q_i\rangle |\text{sgn}(p-q_i)\rangle |j\rangle, \quad (103)$$

where $q_i(j)$ represents the position of the i th occupied qubit in $|j\rangle$. The superposition represented by Eq. (103) corresponds to a subset of (p, q) pairs that serve as the indices to $T(p-q)$ coefficients associated with valid $a_p^\dagger a_q$'s when applied to a η -particle state $|j\rangle$. The O_A oracle then takes $|p-q_i\rangle |\text{sgn}(p-q_i)\rangle$ to retrieve the value of $T(p-q_i)$.

Fig. 23 shows the circuit for block encoding a one-body η -particle Hamiltonian with translational invariance. Notice that, compared to Fig. 18, the additional arithmetic circuit block labeled by SUB is used to generate the superposition of $|p-q_i(j)\rangle$ which is then passed into O_A to retrieve the value of $T(p-q_i)$.

For this type of Hamiltonian, the number of one-body terms is $\mathcal{O}(n\eta)$. However, the number of unique values of the coefficients $T(p-q_i)$ is $2n-1$. Therefore, to obtain a block encoding with ϵ precision, we need

$$m_b = \log\left(\frac{n\eta}{\epsilon}\right). \quad (104)$$

By substituting $L = n\eta$ and Eq. (104) into Eq. (80) and Eq. (81) respectively, we can show that the number of T gates required in the circuit is

$$\mathcal{O}\left(n \log(\eta) + \left\lceil \frac{n}{\lambda} \right\rceil + \lambda \log\left(\frac{n\eta}{\epsilon}\right)\right) \quad (105)$$

and the T-depth of the circuit is

$$\mathcal{O}\left(n \log(\eta) + \frac{n}{\lambda} + 2 \log(\lambda)\right), \quad (106)$$

where $1 \leq \lambda \leq n\eta$.

Compared to the general η particle block encoding with one-body interaction VII, the reduction in optimal gate complexity with this method is $\mathcal{O}\left(\sqrt{n^2 \log\left(\frac{n\eta}{\epsilon}\right)} - \sqrt{n \log\left(\frac{n\eta}{\epsilon}\right)}\right)$, which can be deduced by substituting $L = n^2, m_b = \log\left(\frac{n\eta}{\epsilon}\right)$ and $L = n, m_b = \log\left(\frac{n\eta}{\epsilon}\right)$ into Eq. (65) and taking the difference. It is

significantly larger than the additional cost $\mathcal{O}(\log(n) + \log(\frac{1}{\epsilon}))$ incurred in the subtraction and the comparison oracle.

C. Hamiltonians that can be factorized as products of number operators

If the two-body component of the Hamiltonian in Eq. (20) only contains terms in which $p = r$ and $q = s$, the Hamiltonian can be simplified to

$$\mathcal{H} = \sum_{\substack{p,q=0 \\ p \neq q}}^n V_{pq} n_p n_q, \quad (107)$$

i.e., it can be factorized as a sum of products of number of number operators.

The O_C oracle of the number operator product can be greatly simplified from the O_C for general two-body interaction implementing Eq. (47), discussed in Sec. IV as the product of number operators will not generate phase or bit flips. The SPARSITY oracle O_C for the number operator product $n_p n_q$ where $p \neq q$ satisfies that

$$O_C |0\rangle |p\rangle |q\rangle |j\rangle = |o(j; p, q)\rangle |p\rangle |q\rangle |j\rangle, \quad (108)$$

where $o(j; p, q) = 0$ if $|j_p, j_q\rangle = |1\rangle$ and $o(j; p, q) = 1$ otherwise. To implement the O_C oracle, we employ a SWAP-UP circuit to verify whether both $|j_p\rangle = |1\rangle$ and $|j_q\rangle = |1\rangle$. If this condition is satisfied, the state of the validation qubit is flipped from $|0\rangle$ to $|1\rangle$. This step requires $\mathcal{O}(n)$ T gates and generates a circuit of $\mathcal{O}(\log(n))$ T depth. The O_C oracle and O_A oracle require

$$\mathcal{O}\left(n + \frac{n^2}{\lambda} + \lambda \log\left(\frac{n^2}{\epsilon}\right)\right) \quad (109)$$

T gates and generates a circuit of

$$\mathcal{O}\left(n + \frac{n^2}{\lambda} + \log(\lambda)\right) \quad (110)$$

T depth, which can be deduced by substituting $L = n^2$ and $m_b = \log(\frac{n^2}{\epsilon})$ in Eq. (63) and Eq. (64).

To restrict the block encoding to the η -particle sector of the Hamiltonian, we first generate a superposition of valid indices pair through indirect diffusion for a η particle state,

$$\frac{1}{\sqrt{\eta^2}} \sum_{i_1=0}^{\eta-1} \sum_{i_2=0}^{\eta-1} |i_1\rangle |i_2\rangle |p_{i_1}(j)\rangle |q_{i_2}(j)\rangle |j\rangle, \quad (111)$$

where we use $p_{i_1}(j)$ to represent the bit index of the i_1 th occupied qubit in $|j\rangle$ and $q_{i_2}(j)$ to represent the bit index of the i_2 th occupied qubit in $|j\rangle$. With SWAP-UP circuit to verify whether both $|j_{p_{i_1}}\rangle = |1\rangle$ and $|j_{q_{i_2}}\rangle = |1\rangle$.

Again, if the condition is satisfied, we flip the state of the validation qubit from $|0\rangle$ to $|1\rangle$ and obtain

$$\frac{1}{\sqrt{\eta^2}} \sum_{i_1=0}^{\eta-1} \sum_{i_2=0}^{\eta-1} |o(j; i_1, i_2)\rangle |i_1\rangle |i_2\rangle |p_{i_1}(j)\rangle |q_{i_2}(j)\rangle |j\rangle.$$

Then block encoding to the η -particle sector of Hamiltonian require

$$\mathcal{O}\left(n \log(\eta) + \frac{n^2}{\lambda} + \lambda \log\left(\frac{n^2}{\epsilon}\right)\right) \quad (112)$$

T gates and generates a circuit of

$$\mathcal{O}\left(n \log(\eta) + \frac{n^2}{\lambda} + \log(\lambda)\right) \quad (113)$$

T depth, deduced from Eq. (80) and Eq. (81) with $L = n^2$ and $m_b = \log(\frac{n^2}{\epsilon})$.

D. Examples

In this section, we give a few examples of model Hamiltonians that have special structures and show how techniques discussed above can be used to reduce the gate complexity of the block encoding circuits for these Hamiltonians.

We summarize the gate complexity of block-encoding circuits across different models in Table I, Table II and Table III. In addition, we discuss the complexity for simulating the quantum dynamics with the block encoding we constructed and compare with the cost of other methods simulating the quantum dynamics for η particle state Table IV.

1. Nearest-neighbor Hubbard model

In this section, we examine the block encoding circuit for the nearest-neighbor Hubbard model, which serves as a prototypical many-electron system that captures a variety of correlated-electron phenomena. Its Hamiltonian is given by

$$\mathcal{H} = - \sum_{p,q=0}^{n-1} \sum_{\sigma \in \{\uparrow, \downarrow\}} T(p-q) a_{p,\sigma}^\dagger a_{q,\sigma} + U \sum_{p=0}^{n-1} n_{p,\uparrow} n_{p,\downarrow}, \quad (114)$$

where $T(p-q)$ is non-zero only for nearest neighbors, i.e., when $|p - q| \leq 1$. This model is one special case as discussed in Sec. VIII B and will be referred to as the nearest-neighbor Hubbard Model in Table III.

Because the non-zero coefficients of the one-body term are translational invariant and limited to nearest neighbors on the lattice, we can use techniques discussed in both Sec. VIII A and Sec. VIII B to reduce the gate complexity of the block encoding circuit. A natural question

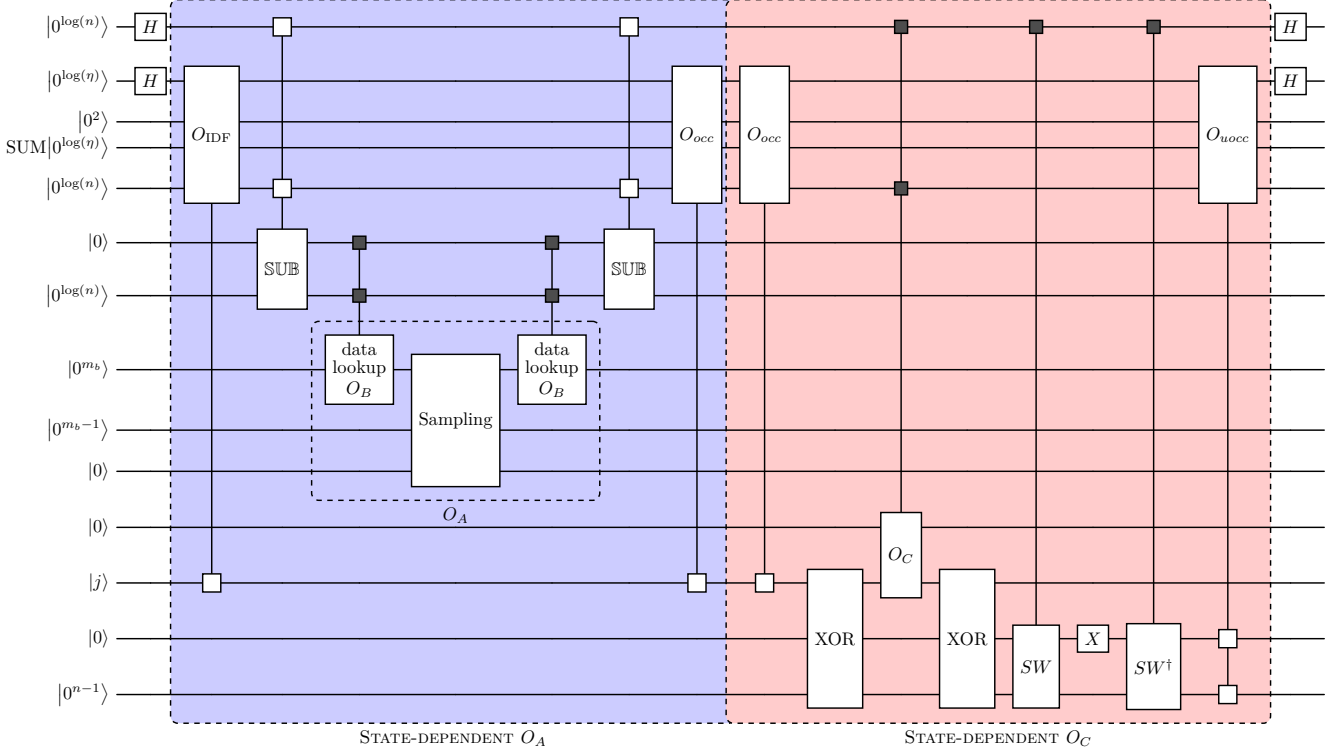


FIG. 23: Quantum circuit of block encoding for one-body η -particle Hamiltonian with translation invariance.

Space	Reference	Qubit	Subnormalization factor	T count	T depth
Full	2018 Babbush et al. [1]	$\mathcal{O}(n + \log(\frac{n}{\epsilon}))$	$\mathcal{O}(n)$	$\mathcal{O}(n + \log(\frac{n}{\epsilon}))$	$\mathcal{O}(n)$
	2018 Kivlichan et al. [2]	N/A	N/A	$\mathcal{O}(n^2 \log(\frac{1}{\epsilon}))$	$\mathcal{O}(n)$
	This paper	$\mathcal{O}(n + \log(\frac{n}{\epsilon}))$	$\mathcal{O}(n)$	$\mathcal{O}(n + \log(\frac{n}{\epsilon}))$	$\mathcal{O}(\log(n))$
η -particle	2021 Tong, An et al. [36]	$\mathcal{O}(n + \log(\frac{n}{\epsilon}))$	$\mathcal{O}(\eta)$	$\mathcal{O}(n \log(n) \log(\frac{1}{\epsilon}))$	$\mathcal{O}(n)$
	This paper	$\mathcal{O}(n + \log(\frac{\eta}{\epsilon}))$	$\mathcal{O}(\eta)$	$\mathcal{O}(n \log(\eta) + \log(\frac{\eta}{\epsilon}))$	$\mathcal{O}(n \log(\eta))$

TABLE III: Comparison of Input model cost for NN Hubbard Model. In the table, n is the number of spin orbitals in the system, and η is the number of particles for the states we consider in the paper. Each row corresponds to the input model constructed in a paper. Note that we use N/A to indicate that the cost is not applicable for the paper [2] as the paper focuses on the quantum simulation with trotterization without a clear construction of the input model.

Model	Reference	T count	Method
General	2018 Babbush et al. [1]	$\mathcal{O}(n^8 + n^4 \log(\frac{n^4}{\epsilon}))$	Qubitization
	This paper	$\mathcal{O}(n^2 \eta^2 [n \log(\eta) + \frac{n^4}{\lambda_1} + \tilde{\lambda}_1 \log(\frac{n^2 \eta^2}{\epsilon})])$	Qubitization
Factorized	2018 Kivlichan et al. [2]	$n \eta^{1+\frac{1}{p}} \cdot n^2 \log(\frac{1}{\epsilon})$	Trotterization
TI Factorized	2018 Babbush et al. [1]	$\mathcal{O}(n^3 + n^2 \log(\frac{1}{\epsilon}))$	Qubitization
	This paper	$\mathcal{O}(n \eta [n \log(\eta) + \frac{n}{\lambda_2} + \tilde{\lambda}_2 \log(\frac{n \eta}{\epsilon})])$	Qubitization
Localized	2018 Babbush et al. [38]	$\mathcal{O}(\frac{n^2 n^3 \log(1/\epsilon)}{\log \log(1/\epsilon)})$	Trotterization
	This paper	$\tilde{\mathcal{O}}(\eta^2 [n \log(\eta) + \frac{n^2}{\lambda_3} \log(\frac{\eta^2}{\epsilon}) + \tilde{\lambda}_3 \log(\frac{\eta^2}{\epsilon})])$	Qubitization

TABLE IV: Comparison of T gate cost for quantum dynamic simulation for second-quantized electronic structure Hamiltonian. The $\tilde{\lambda}_1 \in [1, n^4]$, $\tilde{\lambda}_2 \in [1, n]$, $\tilde{\lambda}_3 \in [1, n^2 \log^2(\frac{\eta^2}{\epsilon})]$ are three free integer parameters used in [43]. We neglect the time t in the complexity analysis as all the bounds scale almost linearly with respect to time.

arises: should we use block encoding with translation invariance and adapt it to the nearest-neighbour interaction, or should we take the reverse approach? Both strategies are reasonable, and the best choice depends on the specific context. As discussed earlier, the detailed resource requirements are determined by factors such as system size, the desired precision ϵ for block encoding, and the parameters of the SELECT-SWAP circuit.

We would like to emphasize that the subnormalization factor of the translation invariant Hamiltonian discussed in Sec. VIII B is $\mathcal{O}(n^2)$, which is significantly larger than subnormalization factor of Hamiltonian with nearest-neighbour interactions $\mathcal{O}(nM)$. This motivates us adapt the block encoding of nearest-neighbour interaction to translation invariant Hamiltonian. A thorough comparison between this method and its reverse approach can be left for future work.

Recall the construction in Sec. VIII A, a key step is generating Eq. (92)

$$\begin{aligned} & \frac{1}{\sqrt{nM}} \sum_{p=0}^{n-1} \sum_{m=1}^M |p\rangle |p-m\rangle |m\rangle |0\rangle \\ & + \frac{1}{\sqrt{nM}} \sum_{p=0}^{n-1} \sum_{m=1}^M |p\rangle |p+m\rangle |m\rangle |1\rangle. \end{aligned}$$

To adapt to nearest-neighbour interactions, we don't need to use amplitude oracle takes $|p\rangle |p-m\rangle$ as input. Instead, we can construct an O_A such that it only takes $|m\rangle |0\rangle$ or $|m\rangle |1\rangle$ to retrieve the value $T(p-q) = T(\pm m)$. The number of data stored in the data lookup oracle equals $L = 2m$ instead of $L = n^2$. Therefore, we require

$$\mathcal{O}\left(n + \frac{M}{\lambda} + \lambda \log\left(\frac{nM}{\epsilon}\right)\right) \quad (115)$$

T gates, as deduced from Eq. (63) with $M = 1$ in this model.

The much reduced number of nonzero coefficients to be considered in the nearest-neighbor Hubbard model also translates directly into a reduced gate count for the block encoding of the diagonal block of the Hamiltonian that corresponds to a fixed η particle count.

We adapt the quantum circuit for nearest-neighbour interactions illustrated in Fig. 21. The sparsity oracle remains unchanged. For the amplitude oracle, owing to the translation invariance of the Hamiltonian, the data lookup oracle only requires as input the state $|m\rangle$, stored in the $\log(M)$ -qubit register, together with the sign \pm stored in the single-qubit auxiliary register. Following the discussion in Sec. VIII A, we adjust the number of classical data to $L = \mathcal{O}(M)$ with $m_b = \log\left(\frac{\eta M}{\epsilon}\right)$, where in this case $M \approx 1$.

By substituting the appropriate values of L and m_b into Eq. (80) and Eq. (81), the η -particle block encoding requires

$$\mathcal{O}\left(n \log(\eta) + \log\left(\frac{1}{\epsilon}\right)\right) \quad (116)$$

T gates and generating a circuit with T -depth of

$$\mathcal{O}(n \log(\eta)). \quad (117)$$

Recall that in our circuit construction, the scaling of T gates is essentially the same as that of Clifford gates, apart from the additional overhead incurred when loading classical data in SELECT-SWAP circuit with Controlled multi-target NOT gate.

Loading these classical data requires $4 \log(1/\epsilon)$ Clifford gates for this model. As a result, both the Clifford gate count and T gate count of the block encoding for this model is

$$\mathcal{O}\left(n \log(\eta) + \log\left(\frac{1}{\epsilon}\right)\right). \quad (118)$$

The subnormalization factors for the one-body interaction and for the multiplication of number operators are $n\eta$ and η^2 , respectively. Consequently, the block encoding for a linear combination of these two interactions has a subnormalization factor of $n\eta$ when $\eta < n$.

2. Molecular Electronic Hamiltonian with localized orbitals

In this section, we show how the techniques presented earlier can be used to construct an efficient block encoding circuit for the electronic structure Hamiltonian of a molecular system in quantized form. We assume molecular orbitals $\{\varphi_\ell\}$ can be localized in space, i.e., for each spin-orbital index ℓ , there exists a vector $\vec{c}_\ell \in \mathbb{R}^3$ (called the center of φ_ℓ) such that,

$$|\varphi_\ell(\vec{r})| \leq \varphi_{\max} \exp(-\alpha \|\vec{r} - \vec{c}_\ell\|), \quad (119)$$

for some φ_{\max} which is a finite upper bound of $|\varphi_\ell(\vec{r})|$ for all ℓ in \mathbb{R}^3 .

A direct consequence of orbital localization is that the two electron integral defined by

$$h_{pqrs} = \int_{\mathbb{R}^3} \int_{\mathbb{R}^3} \frac{\varphi_p^*(\vec{r}_1) \varphi_q^*(\vec{r}_2) \varphi_r(\vec{r}_1) \varphi_s(\vec{r}_2)}{\|\vec{r}_1 - \vec{r}_2\|} d\vec{r}_1 d\vec{r}_2, \quad (120)$$

which are the coefficients of the two-body interaction terms in the second-quantized Hamiltonian can have a small magnitude when the centers of the localized orbitals are far from each other. As a result, it is not necessary to encode all these coefficients to obtain a block encoding with ϵ precision.

If, for each orbital, the number of orbitals that have sufficient overlap with itself is limited to M , then the number of h_{pqrs} we need to consider is limited to $L = n^2 M^2$, which can be significantly less than $L = n^4$ if $M \ll n$. Such a reduction translates directly into a much smaller subnormalization factor as well as the size of m_b required in the data lookup circuit block. In fact, if we

can achieve ϵ accuracy by considering only $L = n^2M$ elements of the h_{pqrs} tensor, m_b can be reduced to

$$m_b = \log \left(\frac{n^2 M^2}{\epsilon} \right) \quad (121)$$

from $m_b = \log \left(\frac{n^4}{\epsilon} \right)$ in the most general case in which no localization of the molecular spin orbitals are considered.

Because the number of electrons for a molecular system is fixed at η , we can further reduce the number of two electron integrals to be considered to $L = \eta^2 M^2$ from $L = n^2 M^2$ because the number of valid creation and annihilation pairs is limited to η . Furthermore, m_b can be reduced to $m_b = \log \left(\frac{\eta^2 M^2}{\epsilon} \right)$ from Eq. (121).

We consider the system has one-dimensional structure, it can be obtained that to have ϵ precision block encoding for full Hamiltonian, it is sufficient to require M of scaling $\mathcal{O}(\log(\frac{n^2}{\epsilon}))$ so that the truncated Hamiltonian has ϵ precision still. For η particle Hamiltonian, we can choose M is of the scaling $\mathcal{O}(\log(\frac{\eta^2}{\epsilon}))$ so that the truncated Hamiltonian has ϵ precision. Then the overall complexity of the block encoding is summarized in Table II and Table II with label Localized.

3. Extended Hubbard model

In the section, we study the block encoding of extended Hubbard model,

$$\mathcal{H} = - \sum_{p,q=0}^{n-1} T_{pq} a_p^\dagger a_q + \sum_{p=0}^{n-1} U_p n_p + \sum_{\substack{p,q=0 \\ p \neq q}}^n V_{pq} n_p n_q. \quad (122)$$

This model is referred as Factorized in tables of the paper. The block encoding of the model can be constructed through the linear combination of block encoding for each type of interaction within the Hamiltonian.

The block encoding for the full Hamiltonian has subnormalization factor $\mathcal{O}(n^2)$ based on the discussion in Sec. VI. In the Hamiltonian, no structure is assumed for T_{pq} , U_p and V_{pq} . As a result, to obtain a block encoding with ϵ precision, it is necessary to have $m_b = \mathcal{O}(\log(\frac{n^2}{\epsilon}))$. The overall complexity of block encoding can be obtained through Eq. (63) and Eq. (64) by substituting

$$L = \mathcal{O}(n^2), \quad m_b = \mathcal{O} \left(\log \left(\frac{n^2}{\epsilon} \right) \right). \quad (123)$$

The block encoding for the η -particle Hamiltonian has subnormalization factor $\mathcal{O}(n\eta)$ based on the discussion in Sec. VII. The overall complexity is obtained through Eq. (80) and Eq. (81) with

$$L = \mathcal{O}(n^2), \quad m_b = \mathcal{O} \left(\log \left(\frac{n\eta}{\epsilon} \right) \right). \quad (124)$$

These complexity are summarized in Table I and Table II with label Factorized.

We further consider extended Hubbard model with one-body interaction translation invariant (referred to as TI Factorized in tables) where

$$\begin{aligned} \mathcal{H} = & - \sum_{p,q} T(p-q) a_p^\dagger a_q + \sum_p U_p n_p \\ & + \sum_{p \neq q} V(p-q) n_p n_p. \end{aligned} \quad (125)$$

We first discuss the block encoding for the full Hamiltonian. The subnormalization factor remains $\mathcal{O}(n^2)$ and the requirement for m_b remain $\mathcal{O}(\log(\frac{n^2}{\epsilon}))$ in order to obtain ϵ precision for block encoding. However, following the discussion in Sec. VIII B, the number of classical data L stored in data lookup oracle scales as $\mathcal{O}(n)$ because of the translation invariance. Then Eq. (63) and Eq. (64) gives the complexity.

The block encoding for the η -particle Hamiltonian has a subnormalization factor $\mathcal{O}(n\eta)$ based on the discussion in Sec. VII. The overall complexity is obtained through Eq. (80) and Eq. (81) with

$$L = \mathcal{O}(n), \quad m_b = \mathcal{O} \left(\log \left(\frac{n\eta}{\epsilon} \right) \right). \quad (126)$$

These complexities are summarized in row “Factorized” of Tables I and II.

IX. CONCLUSION AND FUTURE WORK

In the paper, we construct block encodings for a general second-quantized Hamiltonian with one-body and two-body interactions. Instead of applying multi-controlled gates in the sparsity oracle or amplitude oracle as illustrated in [1, 24, 26], we apply the SWAP-UP gate [3] to sparsity oracle and data lookup to amplitude oracle with direct sampling. To the best of our knowledge, this is the first time SWAP-UP gate and data lookup technique are used in this way.

For a general quantum many-body system with one-body and two-body interactions, we achieve a quadratic improvement in T gate count and improve the constant factor for Clifford gates for the number of interaction terms. Furthermore, we develop a state-dependent sparsity oracle and a state-dependent amplitude oracle such that the block encoding has a smaller subnormalization factor for η particle block encoding. We further adapt the framework to the Hamiltonian with structures. In particular, we consider the Hamiltonian with translation invariance and nearest-neighbour interactions.

The decaying properties will also require a less expensive data lookup cost, as less classical data needs to be prepared. Based on the block encoding we construct, we rigorously measure the complexity of running quantum dynamics for time-independent Hamiltonians. We note

that under the same assumptions for the atomic orbital, quantum dynamics simulation using our η -particle block encoding can match the state-of-the-art method introduced in [38].

Although the framework for general second-quantized Hamiltonians has been established, the complexity of the input model is heavily influenced by the physical structure encoded in the coefficient tensor. Constructing input models with structured coefficients—such as those exhibiting various decay properties or matrix product state representations—will be left for future work. On the other hand, inspired by first quantization, one can represent η -particle states using the occupation addresses of the fermions. This idea has been partially explored in [38, 65], but a systematic development of this approach within the framework of block encoding and data lookup remains an open direction.

Computing Centers, Quantum Utility through Advanced Computational Quantum Algorithms, grant No. DESC0025572 under Contract No. DE-AC02-05CH11231 (LL, CY, SZ). The authors thank Di Fang, Bert de Jong and Yu Tong for their helpful comments and suggestions. Part of the work was performed while DL, CY, SZ, and LL were visiting the Institute for Pure and Applied Mathematics (IPAM), which is supported by the National Science Foundation (Grant No. DMS-1925919). D.L. acknowledges support from the U.S. Department of Energy (DOE) under Contract No. DE-AC02-05CH11231, through the Office of Advanced Scientific Computing Research Accelerated Research for Quantum Computing Program, MACH-Q project. SZ is supported by the National Science Foundation CAREER award (grant CCF-1845125).

ACKNOWLEDGMENTS

This work is supported by the U.S. Department of Energy, Office of Science, Accelerated Research in Quantum

[1] R. Babbush, C. Gidney, D. W. Berry, N. Wiebe, J. McClean, A. Paler, A. Fowler, and H. Neven, *Physical Review X* **8**, 041015 (2018).

[2] I. D. Kivlichan, J. McClean, N. Wiebe, C. Gidney, A. Aspuru-Guzik, G. K.-L. Chan, and R. Babbush, *Physical review letters* **120**, 110501 (2018).

[3] K. Wan, *Quantum* **5**, 380 (2021).

[4] S. Lloyd, *Science* **273**, 1073 (1996).

[5] D. S. Abrams and S. Lloyd, *Phys. Rev. Lett.* **79**, 2586 (1997).

[6] I. M. Georgescu, S. Ashhab, and F. Nori, *Rev. Mod. Phys.* **86**, 153 (2014).

[7] G. H. Low and I. L. Chuang, *Quantum* **3**, 163 (2019).

[8] A. Gilyén, Y. Su, G. H. Low, and N. Wiebe, in *Proceedings of the 51st Annual ACM SIGACT Symposium on Theory of Computing* (2019) pp. 193–204.

[9] D. W. Berry, G. Ahokas, R. Cleve, and B. C. Sanders, *Communications in Mathematical Physics* **270**, 359 (2007).

[10] A. M. Childs and R. Kothari, in *Theory of Quantum Computation, Communication, and Cryptography*, edited by W. van Dam, V. M. Kendon, and S. Severini (Springer Berlin Heidelberg, Berlin, Heidelberg, 2011) pp. 94–103.

[11] G. H. Low and I. L. Chuang, *Physical review letters* **118**, 010501 (2017).

[12] S. Chakraborty, A. Gilyén, and S. Jeffery, in *46th International Colloquium on Automata, Languages, and Programming (ICALP 2019)*, Leibniz International Proceedings in Informatics (LIPIcs), Vol. 132, edited by C. Baier, I. Chatzigiannakis, P. Flocchini, and S. Leonardi (Schloss Dagstuhl – Leibniz-Zentrum für Informatik, Dagstuhl, Germany, 2019) pp. 33:1–33:14.

[13] J. M. Martyn, Z. M. Rossi, A. K. Tan, and I. L. Chuang, *PRX Quantum* **2**, 040203 (2021).

[14] F. Della Chiara, M. Nibbi, Y. Shen, and R. Van Beeumen, *arXiv preprint arXiv:2507.20887* (2025).

[15] D. Camps, L. Lin, R. Van Beeumen, and C. Yang, *SIAM Journal on Matrix Analysis and Applications* **45**, 801 (2024), <https://doi.org/10.1137/22M1484298>.

[16] C. Sünderhauf, E. Campbell, and J. Camps, *Quantum* **8**, 1226 (2024).

[17] Q. T. Nguyen, B. T. Kiani, and S. Lloyd, *Quantum* **6**, 876 (2022).

[18] M. Nibbi and C. B. Mendl, *Physical Review A* **110**, 042427 (2024).

[19] J. Hu, S. Jin, N. Liu, and L. Zhang, *Quantum* **8**, 1563 (2024).

[20] T. Kharazi, A. M. Alkadri, J.-P. Liu, K. K. Mandadapu, and K. B. Whaley, *Quantum* **9**, 1764 (2025).

[21] N. Guseynov, X. Huang, and N. Liu, *Phys. Rev. Res.* **7**, 033100 (2025).

[22] T. Kharazi, A. M. Alkadri, J.-P. Liu, K. K. Mandadapu, and K. B. Whaley, *Quantum* **9**, 1764 (2025).

[23] C. F. Kane, S. Hariprakash, N. S. Modi, M. Kreshchuk, and C. W. Bauer, *Quantum* **9**, 1747 (2025).

[24] D. Liu, W. Du, L. Lin, J. P. Vary, and C. Yang, *arXiv preprint arXiv:2402.11205* (2024).

[25] W. Du and J. P. Vary, *Phys. Rev. A* **108**, 052614 (2023), *arXiv:2304.04838* [nucl-th].

[26] W. Du and J. P. Vary, *arXiv preprint arXiv:2402.08969* (2024).

[27] W. A. Simon, C. M. Gustin, K. Serafin, A. Ralli, G. R. Goldstein, and P. J. Love, *arXiv preprint arXiv:2503.11641* (2025).

[28] H. Lamm, Y.-Y. Li, J. Shu, Y.-L. Wang, and B. Xu, *Physical Review D* **110**, 054505 (2024).

[29] H. Li, H. Ni, and L. Ying, *Quantum* **7**, 1031 (2023).

[30] A. W. Harrow, A. Hassidim, and S. Lloyd, *Phys. Rev.*

Lett. **103**, 150502 (2009).

[31] D. W. Berry, A. M. Childs, and R. Kothari, in *2015 IEEE 56th Annual Symposium on Foundations of Computer Science* (2015) pp. 792–809.

[32] L. Lin, arXiv preprint arXiv:2201.08309 (2022).

[33] A. Gilyén, Y. Su, G. H. Low, and N. Wiebe, in *Proceedings of the 51st Annual ACM SIGACT Symposium on Theory of Computing*, STOC 2019 (Association for Computing Machinery, New York, NY, USA, 2019) p. 193–204.

[34] L. N. Trefethen and D. Bau, *Numerical linear algebra* (SIAM, 2022).

[35] Y. Saad, *Iterative methods for sparse linear systems* (SIAM, 2003).

[36] Y. Tong, D. An, N. Wiebe, and L. Lin, Physical Review A **104**, 032422 (2021).

[37] K. Wan, Quantum **5**, 380 (2021).

[38] R. Babbush, D. W. Berry, Y. R. Sanders, I. D. Kivlichan, A. Scherer, A. Y. Wei, P. J. Love, and A. Aspuru-Guzik, Quantum Science and Technology **3**, 015006 (2017).

[39] Y. Su, D. W. Berry, N. Wiebe, N. Rubin, and R. Babbush, PRX Quantum **2**, 040332 (2021).

[40] F. M. Faulstich, K. D. Stubbs, Q. Zhu, T. Soejima, R. Dilip, H. Zhai, R. Kim, M. P. Zaletel, G. K.-L. Chan, and L. Lin, Physical Review B **107**, 235123 (2023).

[41] D. W. Berry, N. C. Rubin, A. O. Elnabawy, G. Ahlers, A. E. DePrince III, J. Lee, C. Gogolin, and R. Babbush, npj Quantum Information **10**, 130 (2024).

[42] D. Camps, L. Lin, R. Van Beeumen, and C. Yang, SIAM Journal on Matrix Analysis and Applications **45**, 801 (2024).

[43] G. H. Low, V. Kliuchnikov, and L. Schaeffer, Quantum **8**, 1375 (2024).

[44] I. F. Araujo, D. K. Park, F. Petruccione, and A. J. da Silva, Scientific reports **11**, 6329 (2021).

[45] Z. Li, X.-M. Zhang, C. Yang, and G. Zhang, arXiv preprint arXiv:2504.05624 (2025).

[46] X.-M. Zhang, T. Li, and X. Yuan, Physical Review Letters **129**, 230504 (2022).

[47] Y. R. Sanders, G. H. Low, A. Scherer, and D. W. Berry, Physical review letters **122**, 020502 (2019).

[48] M. D. Vose, IEEE Transactions on software engineering **17**, 972 (1991).

[49] S. McArdle, A. Gilyén, and M. Berta, arXiv preprint arXiv:2210.14892 (2022).

[50] D. Malz, G. Styliaris, Z.-Y. Wei, and J. I. Cirac, Physical Review Letters **132**, 040404 (2024).

[51] W. J. Huggins, T. Khattar, and N. Wiebe, arXiv preprint arXiv:2506.00132 (2025).

[52] G. H. Low and I. L. Chuang, Phys. Rev. Lett. **118**, 010501 (2017).

[53] Y. Dong, L. Lin, H. Ni, and J. Wang, Quantum **8**, 1558 (2024).

[54] Y. Dong, X. Meng, K. B. Whaley, and L. Lin, Phys. Rev. A **103**, 042419 (2021).

[55] D. S. Oliveira and R. V. Ramos, Quantum Comput. Comput. **7**, 17 (2007).

[56] R. Raussendorf and H. J. Briegel, Quantum Info. Comput. **2**, 443–486 (2002).

[57] D. Gottesman and I. L. Chuang, Nature **402**, 390 (1999).

[58] E. Bäumer and S. Woerner, Physical Review Research **7**, 023120 (2025).

[59] S. Zhu, A. Sundaram, and G. H. Low, arXiv preprint arXiv:2406.18030 (2024).

[60] D. W. Berry, M. Kieferová, A. Scherer, Y. R. Sanders, G. H. Low, N. Wiebe, C. Gidney, and R. Babbush, npj Quantum Information **4**, 22 (2018).

[61] C. Gidney, N. Shutty, and C. Jones, arXiv preprint arXiv:2409.17595 (2024).

[62] A. Wills, M.-H. Hsieh, and H. Yamasaki, Nature Physics , 1 (2025).

[63] C. Gidney, Quantum **2**, 74 (2018).

[64] D. Gosset, R. Kothari, and K. Wu, arXiv preprint arXiv:2411.04790 (2024).

[65] J. Carolan and L. Schaeffer, arXiv preprint arXiv:2410.04015 (2024).